Copyright Warning & Restrictions

The copyright law of the United States (Title 17, United States Code) governs the making of photocopies or other reproductions of copyrighted material.

Under certain conditions specified in the law, libraries and archives are authorized to furnish a photocopy or other reproduction. One of these specified conditions is that the photocopy or reproduction is not to be "used for any purpose other than private study, scholarship, or research." If a, user makes a request for, or later uses, a photocopy or reproduction for purposes in excess of "fair use" that user may be liable for copyright infringement,

This institution reserves the right to refuse to accept a copying order if, in its judgment, fulfillment of the order would involve violation of copyright law.

Please Note: The author retains the copyright while the New Jersey Institute of Technology reserves the right to distribute this thesis or dissertation

Printing note: If you do not wish to print this page, then select "Pages from: first page # to: last page #" on the print dialog screen

ABSTRACT

INVESTIGATION OF NH_3 AND NO ADSORPTION OVER Cu/SAPO-34 AND Cu/Al_2O_3 CATALYSTS FOR NH_3–SCR SYSTEM

by Basil Rawah

In this study, Copper supported on SAPO-34 molecular sieves or alumina is prepared via an incipient wetness impregnation method for ammonia selective catalytic reduction (NH_3-SCR). These NH_3-SCR catalysts are characterized by pulse chemisorption, temperature-programmed reduction (TPR), and temperature-programmed desorption (TPD) with three different conditions (NH_3, NO, combined NH_3-NO) to evaluate the adsorption of ammonia and nitric oxide. Cu/SAPO-34 catalyst has shown higher ammonia adsorption capacity compared to Cu/Al_2O_3 catalyst. The Cu/SAPO-34 adsorption is enhanced due to the strong acidity and high surface area of SAPO-34 molecular sieves. NO adsorption peaks over both catalysts are small (for NO-TPD) and these peaks become broader when a combined NH_3-NO is introduced to the system.

However, Cu/SAPO-34 & Cu/Al_2O_3 surface area and acidity are decreased dramatically comparing to SAPO-34 and Al_2O_3 supports. These observations are verified by TPR and CO chemisorption. The formation of bulk copper aluminate over (Cu/Al_2O_3) surface and CuO over (Cu/SAPO-34) surface may block the acid sites. Moreover, the metal dispersion over both catalysts is below 10%.

Based on the comparison, various factors could influence the adsorption of NH_3 and NO over the catalyst surface. The high specific surface area could provide abundant adsorption sites, which increase the adsorption capacity. Also, the multiple locations of acid spots along a wide temperature range, which are seen over Cu/SAPO-34, could continuously maintain the adsorption of NH_3 and NO even at elevated temperature.

INVESTIGATION OF NH_3 AND NO ADSORPTION OVER Cu/SAPO-34 AND Cu/Al_2O_3 CATALYSTS FOR NH_3–SCR SYSTEM

by
Basil Rawah

A Thesis
Submitted to the Faculty of
New Jersey Institute of Technology
In Partial Fulfillment of the Requirements for the Degree of
Master of Science in Chemical Engineering

Otto H. York Department of
Chemical, Biological and Pharmaceutical Engineering

May 2017

APPROVAL PAGE

INVESTIGATION OF NH_3 AND NO ADSORPTION OVER Cu/SAPO-34 AND Cu/Al_2O_3 CATALYSTS FOR NH_3–SCR SYSTEM

Basil Rawah

Dr. Xianqin Wang, Thesis Advisor — Date
Associate Professor of Chemical, Biological and Pharmaceutical Engineering, NJIT

Dr. Reginald P.T. Tomkins, Committee Member — Date
Professor of Chemical, Biological and Pharmaceutical Engineering, NJIT

Dr. Robert B. Barat, Committee Member — Date
Professor of Chemical, Biological and Pharmaceutical Engineering, NJIT

BIOGRAPHICAL SKETCH

Author: Basil Sabri Rawah

Degree: Master of Science

Date: May 2017

Undergraduate and Graduate Education:

- Master of Science in Electrical Engineering,
  New Jersey Institute of Technology, Newark, NJ, 2017

- Bachelor of Science in Chemical Engineering,
  King Abdul Aziz University, Jeddah, Saudi Arabia, 2010

Major: Chemical Engineering

This is for my awesome parents, Sabri and Fayza

and for my beloved wife, Rufaida and my son, Hamza

who have always supported me and encouraged me to follow my dreams

ACKNOWLEDGMENT

First of all, I am grateful to my thesis advisor, Dr. Xianqin Wang. I could not complete this thesis without her professional guidance and her patience and being strict with me.

I would also like to express my gratitude to my committee members, Dr. Reginald Tomkins and Dr. Robert Barat for agreeing to be part of my work

In addition, I would like to thank my peer Maocong Hu for training and help during the whole research. Lastly, I take this opportunity to deeply thank my parents, wife and son for their love and understanding and patience.

TABLE OF CONTENTS

TABLE OF CONTENTS
(Continued)

TABLE OF CONTENTS
(Continued)

LIST OF TABLES

LIST OF FIGURES

CHAPTER 1

INTRODUCTION

Growth in the world population brings along with it more modern life demands like energy, transportation, public services and chemical production. According to a recent estimate of worldwide car production, in 2015, around 32 million more cars were produced comparing to car production statistics in 2000. It is about 70% increase in auto manufacturing only within 15 years period [1]. Consequently, this dramatic growth in development can lead to harmful emissions discharged from car exhausts or factory chimneys. These emissions might badly pollute air and the environment. A recent study was conducted by the Organization for Economic Co-operation and Development (OECD) to estimate global energy-related carbon dioxide (CO_2) emissions. Although the current serious efforts to moderate worldwide CO_2 emissions have been implemented, the growth in global CO_2 emissions is projected to increase by one-third from 2012 to 2040 [2]. Therefore, current pace of global development is not sustainable and it is highly urgent to keep up with this rapid growth with new environmental catalytic materials or techniques.

The environmental catalysis can be defined as catalytic processes used to abate pollution and provide clean energy [3]. Emissions from car exhausts and stationary sources like refineries are composed of NO_x, CO and hydrocarbons. Converting these toxic emissions to less harmful emissions like CO_2, N_2 and H_2O is very challenging [4].

Nitrogen oxide (NO_x) is considered a major air pollutant due to its harmful impact on both human health and the environment. NO_x, which is mostly referred to nitrogen monoxide NO and nitrogen dioxide NO_2, contributes to the formation of ground-level or

"bad" ozone, which is very polluting [5]. It is critical to note that the ozone that should be reduced is tropospheric ozone. It is the ozone in the ambient air that we all breathe. Breathing this ozone tends to trigger several health issues like coughing, chest pain, and asthma, the repetitive exposure to this ozone could harm lung functioning or permanently scar its tissues [5, 6]. In addition to issues associated with ozone, sulfur oxides (SO_x) and NO_x in the atmosphere react with moisture and oxygen to form sulfuric and nitric acid. Acid rains along with dry deposition harshly affect the ecosystem, which might cause a negative impact to our economy. Acid rains remove minerals and nutrients from soil where trees and plants need to grow. Moreover, acid rain can leach aluminum from the soil and that aluminum is generally harmful and poisonous to fish and the wildlife [4].

In recent years, there has been an increasing interest in understanding and developing catalytic NO_x abatement. Numerous reviews concerning various aspects of NO_x reduction have been published; some details are discussed in the following sections.

1.1 Nitrogen Oxides (NO_X)

About 80% of the air we breathe is an inert gas, nitrogen (N_2). In this form, it is neutral but the single atom of nitrogen (N) can be reactive and has an ionization level from plus one to plus five [7]. Hence, this nitrogen has the ability to form several oxides. Selected nitrogen oxides, i.e., (N_2O, NO, NO_2, N_2O_3, N_2O_4, N_2O_2, and N_2O_5.) are represented in Table 1.1.

Table 1.1 Properties of Selected Nitrogen Oxides

Formula	Name	Color	State of Matter @(ambient temperature)
N_2O	Nitrous Oxide	Colorless	Gas
NO	Nitric Oxide	Colorless	Gas
NO_2	Nitrogen Dioxide	Red-Brown	Gas
N_2O_3	Dinitrogen Trioxide	Black	Liquid
N_2O_4	Dinitrogen Tetroxide	Transparent	Liquid
N_2O_2	Dinitrogen Dioxide	Colorless	Gas
N_2O_5	Dinitrogen Pentoxide	White	Solid

Source: Clean Air Technology Center, U.S.E.P., *Nitrogen Oxides (NOx), Why and How They Are Controlled*, E. 456/F-99-006R, Editor. 1999.

Dissolving any of these oxides in water forms nitrous acid (HNO_2) or nitric acid (HNO_3). When nitric acid is neutralized, it forms nitrate salts while nitrous acid forms nitrite salts [7].Therefore, NO_x and its different derivatives can react in different form. It can react as gases in the atmosphere, as acids in water droplets or as salts. In fact, all these forms have major contributions to pollution like acid rain.

The three most dominant nitrogen oxides in air are N_2O, NO and NO_2. Nitrous oxide (N_2O), also known as laughing gas, is produced by both natural and human sources. About 95% of the natural source comes from soils under natural vegetation and oceans. Human source of nitrous oxide is mainly emitted from agriculture activity like emissions of N_2O from fertilized agricultural soils and livestock manure [8]. It is an odorless and colorless gas that is used as an anesthetic and analgesic [6]. Nitrous oxide

contributes to ozone destruction in the stratosphere. Also, it is a greenhouse gas that contributes to global warming by holding heat radiating from earth.

NOx emissions from combustions are mainly in the form of NO. The formation of NO from combustion is governed by Zeldovich equations. According to these equations, at a high temperature of 1300 ^{o}C, the generation of NO is limited by oxygen amount in the air. However, at low temperature below 760 ^{o}C, the amount of generated NO is much lower or even the reaction could not happen. In fact, NO generation is a function of air to fuel ratio and it is more prominent on the fuel–lean side of the stoichiometric ratio [7]. The Zeldovich equations are:

$$N_2 + O \leftrightarrow NO + N \quad (1.1)$$

$$N + O_2 \leftrightarrow NO + O \quad (1.2)$$

$$N + OH \leftrightarrow NO + H \quad (1.3)$$

Around 90% of NO emissions are generated by human activity (anthropogenic). Natural emission of NO from soils; lightning and natural fires account for only 10% of total NO emissions [7].

Nitrogen dioxide (NO_2), one of air pollutions gases, is generated as a result of road traffic and other fossil fuel combustion processes. Its presence in air contributes to the formation of additional secondary air pollutants like particulate matter. Also, it plays a major role in the formation of acid rain [9].

Dinitrogen trioxide (N_2O_3) and dinitrogen tetroxide (N_2O_4) concentration in the atmosphere are so minimal, which is why their effects are usually ignored. Moreover,

The NO_2 concentration limits the formation of N_2O_4. Two molecules of NO_2 form a single molecule of N_2O_4.

Dinitrogen pentoxide (N_2O_5) is a dangerous oxidizer, very reactive and unstable. The decomposition of N_2O_5 generates nitric acid (HNO_3). The N_2O_5 concentration in air is very low. Otherwise, it can be generated from a specific designed process from NO production facility [7].

Some experts in this field have different views about which one of these nitrogen oxides should be regulated and have the most attention. Some experts believe that controlling NO_x can be done by reducing NO_2 only due to the rapid conversion of NO to NO_2 and N_2O, N_2O has a long life, is not highly reactive. Others feel that, both NO and NO_2 should be regulated due to their major contribution to ozone formation. Another group believe that all nitrogen oxides should be regulated even less reactive N_2O. Human activities mainly produce NO and NO_2 while the other nitrogen oxides like N_2O is generated naturally. Therefore, both NO and NO_2 should have a priority for controlling [7].

1.2 NO_x Sources

According to the Environmental Protection Agency (EPA), about 50% of NO_x emissions are generated from automobiles and other mobile source. Nearly 40% of the generated NO_x from stationary sources is emitted from electric power plant boilers. NO_x emissions from other anthropogenic sources are incinerators, industrial boilers, reciprocating spark gas turbines, diesel engines and ignition in stationary sources, and petroleum refineries [10]. Natural sources (biogenic) of NO_x, such as forest fires, lightning, grass fires, bushes, trees, yeasts and grasses, produce different amounts of NO_x. The following graph,

Figure 1.1 shows the amount NO_x produced from anthropogenic sources.

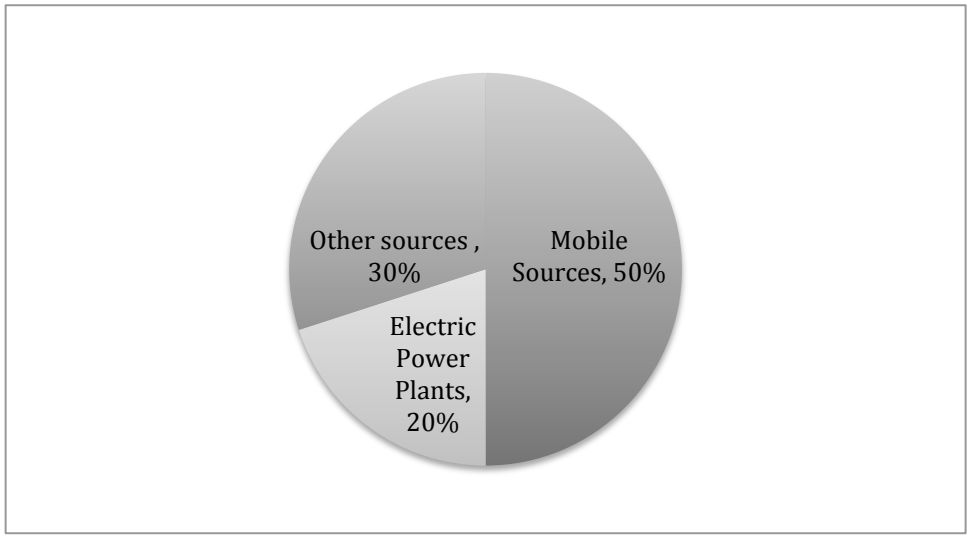

Figure 1.1 Amount NO_x produces from anthropogenic sources.

Source: Clean Air Technology Center, U.S.E.P., *Nitrogen Oxides (NOx), Why and How They Are Controlled*, E. 456/F-99-006R, Editor. 1999.

From the NO_x emission graph (Figure 1.1), the two categories for mobile and stationary sources are about 70% of total emissions and should be reduced. However, these two categories cannot be reduced to zero. We do not expect cars, buses and other core essential transportations to disappear. Zero-emission cars are still in development and we expect that it is too soon to be in the marketplace. Moreover, the idea of shifting from the fossil fuel engine to electric engine cars takes time. The community has to be familiar and knowledgeable about the new technology before starting use it.

According to Bosch and Janssen [7] NO_x formed during the combustion process can be categorized into three types. Moreover, NO_x from engine exhaust typically consists of a mixture of 95% NO and 5% NO_2. The first category is called thermal NO_x. In this type, NO_x is formed due to the oxidation of N_2 at high temperature. The combustion temperature (above 1300 °C) and the molar concentrations of both nitrogen

and oxygen control the concentration of thermal NO_x.

$$N_2 + O_2 \leftrightarrow 2NO, \quad \Delta H^0_{298} = 180.6\ kJ/mol \tag{1.4}$$

Fuel NO_x is the second category. The oxidation of nitrogen in fuel such as coals or heavy oils creates fuel NO_x. Unlike thermal NO_x, the formation of NO_x is independent of the combustion temperature [4]. The third category is called prompt NO_x. In this category, several steps rule nitrogen oxides generation. First, the atmospheric nitrogen reacts with hydrocarbon fragments to produce HCN and H_2CN, which can be oxidized to form NO. Then, further oxidation of NO generates both NO_2 and N_2O as shown below.

$$NO + 1/2O_2 \leftrightarrow NO_2, \quad \Delta H^0_{298} = -113\ kJ/mol \tag{1.5}$$

$$2NO \leftrightarrow N_2O + 1/2O_2, \quad \Delta H^0_{298} = -99\ kJ/mol \tag{1.6}$$

The formation of prompt NO_x is proportional to the amount of carbon atoms existing per unit volume. Also, it can be formed in an acceptable amount even at low temperature, fuel-rich conditions and at short residence time.

1.3 NO_X Emissions in Mobile Diesel Cars

As seen in Figure 1.1, approximately 50% of NO_x emissions from human activities is generated from the automobile sector. Moreover, mobile applications commonly are based on either gasoline engines or diesel engines. Because of the difference in concept and technology between these two engines, the tail pipe emissions are also varied in

composition. According to Table 1.2, the overall NO_X emission rates for diesel cars are much bigger than gasoline cars. In fact, Euro 3 diesel vehicles showed 5.5 times higher NO_x average emission than Euro 3 gasoline vehicles. Moreover, Euro 4 mobile diesel engines demonstrated 12.5 times higher NO_x average emission than Euro 4 mobile gasoline engines at the same operating conditions.

Our study is focused on reducing NO_X from diesel engines only because these engines produce more NO_X than the gasoline engines. Understanding how the diesel engine works and identifying and quantify the released emissions would help to design a suitable technology to reduce the undesirable products.

Table 1.2 NO_x Emissions From Gasoline and Diesel Vehicles

No.	Engine type	Technology	NO_X emission rates (g/km)
1	Gasoline	Euro 3	0.015−0.27
2	Gasoline	Euro 4	0.013−0.1
3	Diesel	Euro 3	0.45−1.1
4	Diesel	Euro 4	0.31-1.1

Source: Adapted from Table 1, Figures 6, 10 and 11 of Lozhkina et al.

1.3.1 Diesel Engine (Heavy-Duty Vehicle)

Diesel engines have remarkable features that make them the most preferred engines for heavy-duty vehicles. The diesel engine is reliable, efficient and durable, and it has a low operating cost. Thus, this engine has numerous applications compared to gasoline engines. It is the main power source for the commercial transportation buses, trains, and ships and even off-road industrial vehicles such as mining machines. Alternatively, this

combustion engine, using hydrocarbons, has a major contribution to some environmental issues. High amounts of particulate matter (PM) and NO_x are emitted from diesel exhaust gas. These two severely affected the environment as well as caused health problems. Health experts have discovered certain effects of diesel engine emissions, such as causing lung damage and respiratory problems. Also, some experts think that there is a correlation between cancer and diesel emissions. Furthermore, acid rains, ground-level ozone or reducing visibility are also caused by these emissions too [10].

1.3.2 Operation and Emissions of Heavy Duty Diesel Engines

The mixture of fuel and air is auto-ignited inside the engine. The high compressed air inside the combustion chamber generates a high temperature that helps injected diesel fuel inside the cylinder to ignite spontaneously. As a result of this combustion, a chemical energy in a form of heat is released and then converted to a mechanical force.

Since diesel fuels are extracted from fossils, diesel fuel consists of carbon and hydrogen. Theoretically, the complete combustion of diesel fuels generates only CO_2 and H_2O. However, in reality, the complete combustion does not happen. Several reasons, such as the air to diesel ratio, combustion temperature and ignition inhibit the complete combustion. The major issues that are produced from the incomplete combustion are NO_x, CO, PM and HC [10].

1.3.3 Heavy-Duty Diesel Engine Legislation and Regulations

Due to the harmful impact of NO_x emissions on the environment and other related health issues, regulations and restrictions have been proposed to reduce NO_x emissions. These regulations might vary from one country to another in terms of types or levels, but the main purpose is to reduce NOx to an acceptable level.

In the United States, EPA has introduced the first federal emission limits to control CO, HC and NO_X in ~1974. Due to the rapid growth of automobile production, this emission standard has gradually tightened up during the following decades. From Table 1.3, the mandatory amount of NO_x emissions was 4 g/bhp.hr in 1998, which is about 60% less than the limited amount in the previous years. Nowadays, the NOx emission has become even more restricted. The emitted NO_x should be equal or below 0.2 g/bhp.hr [11].

In Europe, a similar regulation has been tightly used since 1992. As shown in Table 1.3, the first EU Emission Standards for heavy-duty diesel engines (Euro I) aimed to reduce NOx emission to 8 g/kWh. In fact, every 2 to 4 years period, EU introduces new updated emission standards like Euro II, Euro V and Euro IV to meet or exceed the quality requirements of the surrounding air. For instance, the new emission standard (Euro VI), limiting NOx reduction to 0.4 g/kWh for every heavy-duty diesel engine, has been employed after 2013. The goal of these firm restrictions is to sustainably adapt with the huge growth in diesel engine applications [11]

Table 1.3 Emission Standards for Heavy-Duty Engines in The U.S and Europe

US EPA & California Emission Standards for Heavy-Duty CI Engines, g/bhp·hr				
Year	CO	HC	NO_X	PM
1974	40	–	–	–
1998	15.5	1.3	4.0	0.1
2015	15.5	0.14	0.02	0.01

EU Emission Standards for Heavy-Duty Diesel Engines: Steady-State Testing, g/kWh					
Stage	Date	CO	HC	NO_X	PM
Euro I	1992	4.5	1.1	8.0	0.612
Euro III	2000	2.1	.66	5.0	0.10
Euro VI	2013	1.5	0.13	0.4	0.01

Source: Adapted from Table 1, US EPA & California Emission Standards for Heavy-Duty CI Engines and Table.1 from EU Emission Standards for Heavy-Duty Diesel Engines: Steady-State Testing, www.dieselnet.com/standards.

1.4 NO_X Abatement for Diesel Cars

The worldwide NO_x emission regulations and legislations have pushed scientists to design various emission control technologies. For instance, three-way-catalyst (TWC) technology for gasoline engines is a robust emission control technique due to its immediate removal of CO, C_xH_y and NO_x while its main reaction is the reduction of NO by CO [12]. Moreover, TWC is very effective way to remove 95% of gasoline engine emissions [4].

Since TWC requires fuel-rich conditions to remove NO_X, integrating TWC into diesel cars is ineffective [13]. As explained before, diesel engine operation requires a high amount of oxygen in the fuel gas to effectively perform the combustion. Thus, TWC does not reduce NO_X in diesel engine cars. In the last decade, various alternative post-

combustion methods were introduced to reduce NO_X under lean-burn conditions. Among these aftertreatment technologies, selective catalytic reduction (SCR) technology demonstrates remarkable deNO_X efficiency and can meet with the new emission regulations, which makes SCR technology the dominant lean NO_x aftertreatment compared to other technologies [14].

1.4.1 Selective Catalytic Reduction (SCR)

The SCR process is a reliable technology for reducing NO_X emissions [15]. The process requires a reducing agent and an active catalyst. The reducing agent is added to the gas flue containing NO_X while the catalyst promotes the NO_X reduction by the reducing agent [16]. The SCR technology has a great deNOx efficiency with high selectivity toward N_2 [16]. In addition to these advantages, the SCR has a durable performance with wide operating temperature, affordable cost and available infrastructure [17, 18].

Alongside the different reducing agents, ammonia (NH_3) is a strong reductant for NO_X and it has been integrated into various stationary and mobile diesel engine applications in the last 20 years [19]. Basically, NH_3 is chemisorbed onto the active sites of the catalyst surface where the reaction of NH_3 with the adsorbed NO_X from the flue gas occurs. NH_3 has different sources depending on applications. It can be in a form of ammonium carbamate, dissolved urea in water, solid urea or liquefied ammonia [16].

1.4.2 Urea-Selective Catalytic Reduction (NH_3-SCR) Chemistry

As both safety and toxicity are concerned, urea has been selected as a reducing agent for mobile SCR diesel engines. Understanding the urea mechanism as a reducing agent and its role to reduce NO_X, profoundly helps optimizing the SCR operation conditions. In

mobile applications, urea is generally stored as an aqueous solution that is sprayed into the hot exhaust gas stream. As a result, it is decomposed into ammonia (NH_3) through three steps: evaporation, thermal decomposition and HNCO hydrolysis. The following reactions illustrate the above steps in details [20].

First Step: non-catalytic evaporating of water from urea droplets changes the urea phase to a melted one (molten urea).

$$NH_2 - CO - NH_{2\,(aq)} \rightarrow NH_2 - CO - NH_{2\,(s)} + H_2O_{(g)} \quad (1.7)$$

Second Step: thermal decomposition of molten urea; this solid urea is thermally decomposed (without catalyst) to ammonia (NH_3) and isocyanic acid (HNCO).

$$NH_2 - CO - NH_{2\,(s)} \rightarrow NH_{3\,(g)} + HNCO_{(g)} \quad (1.8)$$

Isocyanic acid is converted to NH_3 and CO_2 gases through a hydrolysis using water vapor formed from the combustion process.

Third Step: hydrolysis of Isocyanic acid to form NH_3 and CO_2.

$$HNCO_{(g)} + H_2O_{(g)} \rightarrow 2NH_{3\,(g)} + CO_{2\,(g)} \quad (1.9)$$

The overall reaction of urea decomposition to ammonia and carbon dioxide is presented in the following reaction.

$$CO(NH2)2 + H_2O \rightarrow 2NH_3 + CO_2 \quad (1.10)$$

According to reaction (1.10), every mole of urea produces 2 moles of ammonia. From the standard SCR reaction, the stoichiometric molar ratio of NH_3: NO is 1:1. Thus, from the stoichiometric balance, the urea: NO stoichiometric molar ratio is 1:2.

Due to the fact that more than 90% of NOx emissions from diesel exhaust are in a form of NO, the main SCR reaction will be written as the following.

$$4NH_3 + 4NO + O_2 \rightarrow 4N_2 + 6H_2O \quad (1.11)$$

Equimolar amounts of NH_3 and NO with the presence of oxygen are needed to convert NO to N_2 and H_2O. In fact, the absence of oxygen makes the SCR reaction much slower as seen in reaction [1.12] and it does not occur in lean combustion gases.

$$4NH_3 + 6NO \rightarrow 5N_2 + 6H_2O \quad (1.12)$$

However, the presence of NO_2 with NO and ammonia makes the reaction rate much faster than the main SCR reaction.

$$4NH_3 + 2NO + 2NO_2 \rightarrow 4N_2 + 6H_2O \quad (1.13)$$

If NOx emissions are in a form of NO_2 only, the reaction will be much slower than reaction [1.11] and [1.13].

$$8NH_3 + 6NO_2 \rightarrow 7N_2 + 12H_2O \quad (1.14)$$

Regarding the undesired or side reactions, as the temperature rises beyond 400 °C, the nitrous oxide (N_2O) could be formed according to the following reaction.

$$4NH_3 + 4NO + 3O_2 \rightarrow 4N_2O + 6H_2O \quad (1.15)$$

If the temperature increases above 500 °C, NH_3 oxidizes to NO. This undesirable oxidation limits the maximum conversion of NO_x.

$$4NH_3 + 5O_2 \rightarrow NO + 6H_2O \quad (1.16)$$

The ammonia oxidation sets the upper temperature limit for the SCR reaction. However, the formation of ammonium nitrate (NH_4NO_3) at temperature below 200 °C sets the lower temperature limit for the reaction. Ammonium nitrate is generated from the reaction of NH_3 with NO_2 as seen below.

$$2NH_3 + 2NO_2 \rightarrow NH_4NO_3 + N_2 + H_2O \quad (1.17)$$

1.5 NH_3-SCR Catalysts and Deactivation Issues

1.5.1 Common Active Catalysts for NH_3-SCR

The Catalyst is a significant part of the process and many recent studies have focused on the enhancement of the catalytic activity. Basically, NH_3-SCR catalysts can be either metal or metal oxides supported onto different materials like alumina, zeolite, TiO_2 and SiO_2. For instance, Cu/Al_2O_3 is one of the SCR catalysts. This type of catalyst has a very limited practical application due to its moderate NO conversion and narrow operating temperature window. Generally, Cu/Al_2O_3 catalysts have large to medium pore size featured by low specific surface area and broad pore size distribution, which contributes to the poor catalyst performance [21]. Thus, operating temperature, deNOx efficiency, selectivity and sustainability are important to make catalysts efficient for broad applications [22].

One reliable and robust catalysts for SCR reaction is titanium dioxide (TiO_2) supported vanadium oxide (V_2O_5) catalyst, so called V-SCR. Due to the excellent performance as well as affordable price, this catalyst has been used widely for stationary and mobile sources [23]. The commercial V-SCR catalyst (V_2O_5–WO_3/TiO_2) has demonstrated high NO_X reduction activity at a moderate temperature range (300 – 450 °C) with a remarkable sulfur poisoning resistance. A recent study was focused on enhancing V-SCR low temperature catalytic activity [24]. The modified V-SCR catalyst with cerium (Ce) and antimony (Sb) exhibited a decent low temperature NH_3-SCR activity with 90% NO conversion in the temperature range between 210 to 400 °C. For these reasons, V-SCR catalysts might rule the SCR catalyst market in the sense that ultra-low sulfur diesel is still not spread globally.

However, the major drawback of vanadium, which poses threats to human health, is the release of toxic vanadium compounds at high temperature above 600 °C. In fact, the exposure to vanadium pentoxide (V_2O_5) could possibly cause cancer as it is listed as a carcinogen by the International Agency of Research on Cancer (IARC) [25]. Also, the narrow operating temperature window (300 – 450 °C) could be a serious problem, when the SCR unit is attached as a source of high heat.

Therefore, new eco-friendly catalysts with high SCR performance and wide operating temperature are required especially for mobile application. Amongst new emerging SCR catalysts for mobile applications, metal supported zeolites draw much attention due to their durability, high deNOx activity and a broad operating temperature window [26]. From a wide list of active catalysts, copper zeolites seem to be specifically interesting and have been widely studied.

In fact, the properties of both support (zeolite) and the active metal (Cu) in a copper zeolite SCR catalyst have a significant influence on the SCR reactions [27]. Zeolite is one of the molecular sieve materials, which has a uniform porous structure. This type of structure provides a large surface area allowing low concentrated NO_X and NH_3 to adsorb on its surface. Another important feature is that Brønsted acid sites generated from the tetrahedral aluminum centers in zeolite can trigger the formation of NH_4^+ ions from the adsorbed NH_3 which is assumed to be a key step in the reaction mechanism of SCR [28]. Also, the tetrahedral aluminum centers are able to hold Cu cations, allowing these cations to atomically disperse inside the zeolite pores. It is believed that the highly dispersed Cu ions can trigger NO oxidation via a redox cycle. In fact, the feasible NO oxidization and the generation of NO_X adsorption surface centers on

the catalyst is another key step in the reaction mechanism of SCR [27, 29, 30]. Both Cu sites and the Brønsted acid sites in a copper zeolite catalyst permit the reaction between the adsorbed NO_X and NH_4^+ to generate N_2 with a remarkable selectivity [27, 28]. Thus, the Cu/zeolites are bi-functional catalysts offering redox and acidic functions for SCR reactions, which are important for optimizing the SCR activity.

Cu/ZSM-5 (medium pore support with MFI structure) is one of the best Cu/zeolites NH_3-SCR catalysts that has been studied extensively. It has a superior deNOx activity and selectivity of N_2 at a moderate temperate window (200–400 °C) [31]. However, the lack of hydrothermal stability limits its commercial application For instance, mobile diesel emission control requires a durable catalyst that can endure high temperature operation above 670 °C [32].

Recently, other Cu/zeolite systems have been discovered to work as NH_3-SCR catalysts with significant improvements. The (small pore support with CHA structure) catalysts, Cu/SSZ-13 and Cu/SAPO-34, show a remarkable high hydrothermal stability and activity of NH_3-SCR reactions [33]. In a recent study, both Cu/SSZ-13 and Cu/SAPO-34 are able to maintain the optimum deNOx activity about 90-100% at temperatures between (250–450 °C), even after hydrothermal aging at 800 °C with high NO_X conversion [34, 35]. Both SAPO-34 and SSZ-13 have the same CHA structure but with different chemical elements. Unlike SSZ-13, whose framework is built from aluminasilicate structures with Al and Si as the tetrahedrals, the SAPO-34 framework is created by the replacement of Si in the AlPO structure that was originally formed by P [36]. As a result, both reaction and deactivation mechanism are different. The main focus in our study is on SAPO-34 because its mechanisms are still unclear.

1.5.2 Catalyst Deactivation and Issues

The catalyst stability under rough conditions is so crucial especially for automobile applications due to the strict emission rules and regulations. For the NH_3-SCR technology, the catalyst is deactivated either from thermal or chemical degradation mechanisms [37, 38]. High temperature operating conditions could deactivate the catalyst by sintering the metal active sites and reducing the catalyst support surface area. On the other hand, the strong chemisorption of impurities and poisons on catalyst active sites blocks the pores and this causes a loss of surface area leading to a deactivation issue [37, 38]; thus, a huge decrease in deNOx efficiency along with the generation of undesired by products [39].

The loss of catalyst activity due the thermal deactivation might be permanent making the hydrothermal stability so crucial in NH_3-SCR catalyst design. In fact, the SCR catalyst materials could repeatedly be exposed to high temperature operation usually between 600 and 700 °C, since the diesel particulate filter (DPF) is often placed upstream close to the SCR [40].

The NH_3-SCR catalyst is chemically deactivated either by oil or fuel derived impurities or some deposited components from the upstream units. In general, impurities like magnesium, zinc and calcium originate from different additives like detergent, corrosion inhibitors and antioxidant in the engine lubricating oil. These impurities can block the active sites by accumulating on the catalyst surface area causing a drop in catalytic activity [41, 42].

Catalyst poisoning via sulfur is one of the critical issues that can deactivate the SCR catalyst. This problem will remain since sulfur is still present in the burning fuels even at ultra low sulfur levels [16]. In fact, sulfate species are formed over the catalyst

active sites causing a reduction of NO_x conversion [43]. In a typical SCR application process, the flue gas containing SO_2 in the presence of NH_3 causes formation of ammonium sulfate [44]. These species can block the catalyst support pores resulting a significant decrease in the surface area.

In this study, we will investigate the adsorption of NH_3 and NO over copper supported on Al_2O_3 or SAPO-34 catalysts via temperature-programmed desorption (TPD), temperature-programmed reduction (TPR), CO chemisorption characterization experiments. Examining the effect of catalyst support on the adsorption process is important especially for the ammonia-SCR reaction where the ammonia is used as a reductant agent.

CHAPTER 2

Cu/Al_2O_3

2.1 Aluminum Oxide (Al_2O_3)

Alumina (Al_2O_3), also called aluminum oxide, a white non-porous crystalline substance, serves as a support for the SCR catalyst [45]. There are different grades of alumina depending on the application. For catalytic purposes, the high purity (> 99.8) alumina is needed because it provides both strength and stability at high temperature application with a moderate specific surface area, usually as much as 130 m^2/g [45].

The crystal structure of Al_2O_3 is a corundum structure. It is consisted of close packed planes of large anions of oxygen with a radius of 0.14 nm that are set in the order as seen in Figure 2.1. The oxygen anions have (-2) valence while the aluminum cations with a shorter radius, 0.053 nm have valence of (+3). Ideally to maintain the neutral state, there is only a pair of Al^{+3} ions for every three O^{-2} ions. Consequently, two thirds of the octahedral sites of the basic array are occupied via cations [46].

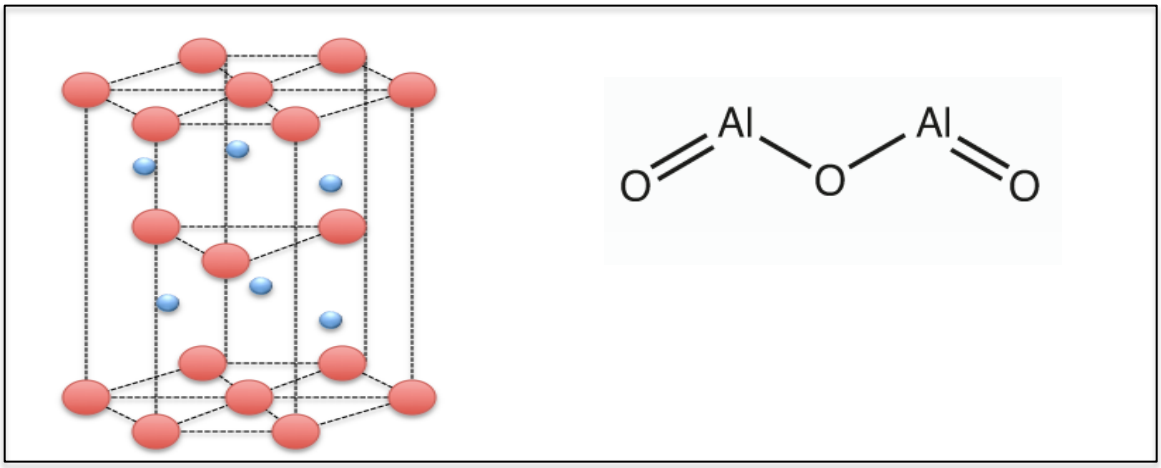

Figure 2.1 Corundum structure of Al_2O_3

Source: Shirai, T., et al., Structural properties and surface characteristics on aluminum oxide powders. 2010.

2.2 Cu/Al_2O_3

Concerning reducing NO_X via a SCR system, Cu supported on an alumina catalyst has shown a reliable activity in practical applications [47]. Previous studies have proven Cu/Al_2O_3 had catalytic activity for NH_3-SCR at a temperature window between 250 to 400 °C. [48] Other studies related to another SCR system, hydrocarbon selective catalytic reduction (HC-SCR), have investigated NO removal on the same catalyst. This study showed that the Cu/Al_2O_3 catalyst has shown a better hydrothermal stability and NO_X conversion for a wide temperature range [49]. Thus, understanding the nature and reactivity of the adsorption phases on the Cu/Al_2O_3 surface is crucial. Moreover, the catalyst synthesis method, copper content, and alumina source significantly affect the catalyst activity. In our study, all the parameters regarding catalyst synthesis and the related characterization tests are explained in the following subsection.

2.3 Preparation of Cu/Al_2O_3

A total of 4.2 wt% of Cu loading was impregnated onto the Al_2O_3 support (Aerosol, Evonik) via an incipient wetness impregnation method. More specifically, 1.06 g of Cu $(NO_3)_2 \cdot 2.5H_2O$ was dissolved in 4.5 mL (which is equal to the impregnating volume of alumina) of deionized water to prepare the Cu $(NO_3)_2$ solution. Then, the solution was added to 4.8 g of the support (Al_2O_3) drop by drop until the impregnating volume was reached. The resulting mixture was dried in the oven at 110 °C for 30 min to avoid the diffusion of Cu inside the alumina pores. The sample was placed in a muffler oven at 110 °C for 12h and then calcined at 550 °C for 5 h. The calcined sample was ground and sieved to 40–80 mesh. The 4.2 wt.% Cu/Al_2O_3 was labelled as Cu-Alu. On the other

hand, the reference sample (labelled as Ref-Alu) was prepared using the same procedure but without adding the copper.

2.4 Catalyst Characterization

2.4.1 Temperature-Programmed Reduction with Hydrogen (H_2-TPR)

H_2-TPR experiments were carried out with an Autochem II 2920 (Micromeritics, USA). Various effluents including H_2, H_2O and O_2 were measured using a mass spectrometer (Stanford Research Systems, Inc., QMS series gas analyzers). 150 mg of catalyst sample was loaded into a U-type quartz tube reactor. This sample was pre-treated in helium with a flow rate of 50 mL/min at 120 °C for 30 min to purge the residual gases and remove moisture. After the catalyst was cooled down to room temperature, H_2-TPR was performed in a 10 vol.% H_2/Ar gas flow at 50 mL/min with a heating rate of 10 °C/ min to 550 °C.

2.4.2 Temperature-Programmed Desorption for NH_3, NO and Combined NH_3-NO

NH_3-TPD and NO-TPD experiments were performed in the same instrument as H_2- TPR, equipped with a mass spectrometer (QMS series gas analyzers) to record the species signals. Prior to TPD experiments, 150 mg of samples were pre-treated in dry helium at a flow rate of 50 mL/min at 120 °C for 30min, and then cooled down to room temperature (23 °C). Then a H_2-TPR experiment was performed in a 10 vol.% H_2/Ar gas flow of 50 mL/min at a heating rate of 10 °C/ min to 400 °C to reduce the sample. Then, after the sample was cooled down again to room temperature, the catalyst was exposed to 10% NH_3/He or 10% NO/He at a rate of 50 mL/min for 20 min, respectively, and then purged with dry He at a flow rate of 50 mL/min for 30 min to remove physically adsorbed

ammonia or adsorbed nitric oxides. Desorption was performed in a He flow with a rate of 10 °C/min to 600 °C for both NH_3-TPD and NO-TPD.

An NH_3-NO-TPD experiment followed the exact steps for NH_3-TPD except for the gas exposure part. After the sample was reduced and then cooled down to room temperature, the sample was first exposed to 10% NH_3/He for 10 min followed by an exposure to 10% NO/He for 10 min.

2.4.3 Pulse Experiment

CO pulse experiments were carried out with the Autochem II 2920 (Micromeritics, USA). About 150 mg of catalyst was loaded into a U-type quartz tube reactor. Prior to pulse CO, the sample was reduced with 10 vol.% H_2/Ar gas flow of 50 mL/min at a heating rate of 10 °C/ min at 500 °C for 30 min. The catalyst was subsequently flushed with pure He at a flow rate of 50 mL/min for 30 min. After that, a pulse of 10 vol.% CO/He was introduced into a flow of pure He (20 doses or less) at room temperature. The active particle diameter and the metal dispersion percentage were calculated from the chemisorption result.

2.5 Results and Discussion

2.5.1 Catalyst Dispersion (CO Pulse Experiments)

The catalyst dispersion was measured via a CO chemisorption method. Table 2.1 provides the metal dispersion and crystallite size of a sample Cu-Alu. The metal dispersion was about 8% for the sample Cu-Alu, low metal dispersion. This observation indicates that not all Cu species are in a form of fine crystallites. Agglomerated or bulk Cu on the surface could happen too. The average active particle diameter further reinforces the above observation. Cu-Alu is found to contain moderate size of copper particles of 12.68 nm. In fact, as the catalyst particle size increases, more and more copper species could come together thus forming bulk aluminate or oxide species (CuO).

Table 2.1 Details of Cu Dispersion, Cu Particle Size

Sample	Metal dispersion (%)	Active Particle Diameter (nm)
Cu-Alu	8	12.68

2.5.2 H_2-TPR Analysis

In order to explain the nature of copper species in our Cu/Al_2O_3 catalyst, the H_2 -TPR experiment was conducted. The reduction profile of the catalyst prepared via incipient wetness impregnating method is shown in Figure 2.2. The single reduction peak was observed between 170–230 °C, with a maximum sharp peak centered at 209 °C.

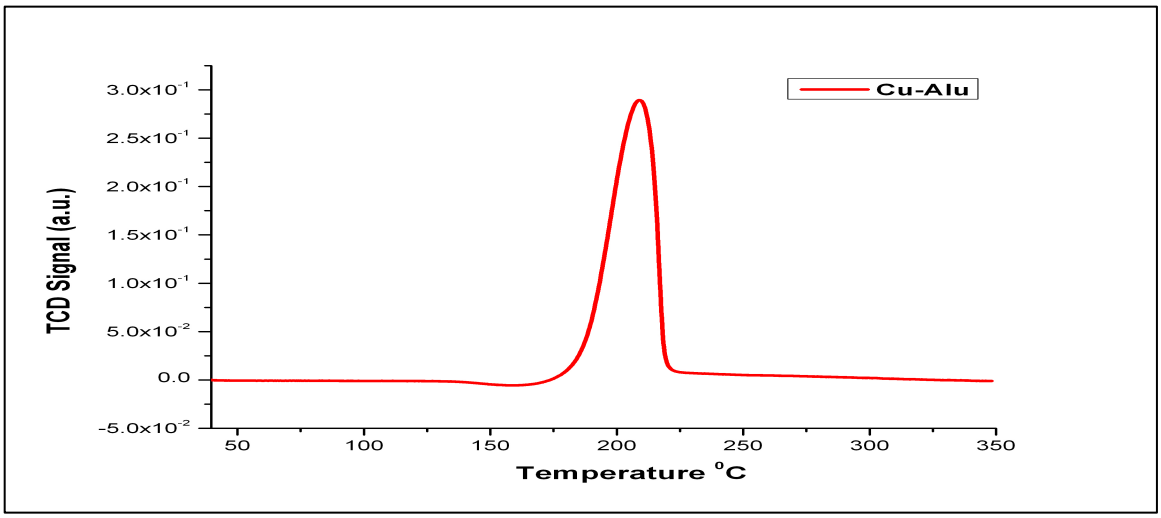

Figure 2.2 Temperature-Programmed Reduction (TPR) for Cu-Alu catalyst.

Different studies [50] reported three different copper species that can be formed on alumina. These are isolated Cu^{2+} ions, a copper aluminate surface phase and crystalline CuO. The first two, isolated Cu^{2+} ions and a copper aluminate surface phase ($CuAl_2O_4$) have the same chemical bonds and are different from the crystalline CuO bonds [50]. It should be mentioned that the surface copper aluminate phase is different from bulk $CuAl_2O_4$. Comparing to the bulk, a surface copper aluminate phase is well dispersed and more active because the main part of Cu^{2+} ions are octahedrally coordinated which is more (energetically) favorable to form six bonds [51]. On the other hand, in the bulk $CuAl_2O_4$ about 60% of the copper ions are in tetrahedral coordination (four bonds) and 40% in octahedral coordination (six bonds) and that is less active than the surface copper aluminate phase [51].

Another study [52] assigned the single peak at low temperature to the reduction of the surface copper aluminate phase in the sense that the isolated Cu^{2+} ions are not active over the alumina and no studies have ever noticed their activity over the Al_2O_3 surface. Others [53] concluded that the low temperature reduction peak was related to CuO. CuO

needs a high temperature at around 270 °C or above to be reduced. Thus, in our case, the TPR results are consistent with these findings in which the reduction peak could be corresponding to the surface copper aluminate phase. However, it might not be uniformly dispersed and the bulk copper aluminate could exist according to the CO pulse results.

2.5.3 NH_3-TPD Surface Acidity

NH3-TPD profiles are shown in Figure 2.3 and Table 2.2 shows ammonia peak area for both samples.

There is a NH_3 desorption peak between 60 and 350 °C with a peak area of 0.52 on Al_2O_3, indicating that the support (Al_2O_3) has a moderate surface acidity and it was able to adsorb NH_3. This finding is in agreement with various studies with pure or modified alumina as a catalyst support [54-56].

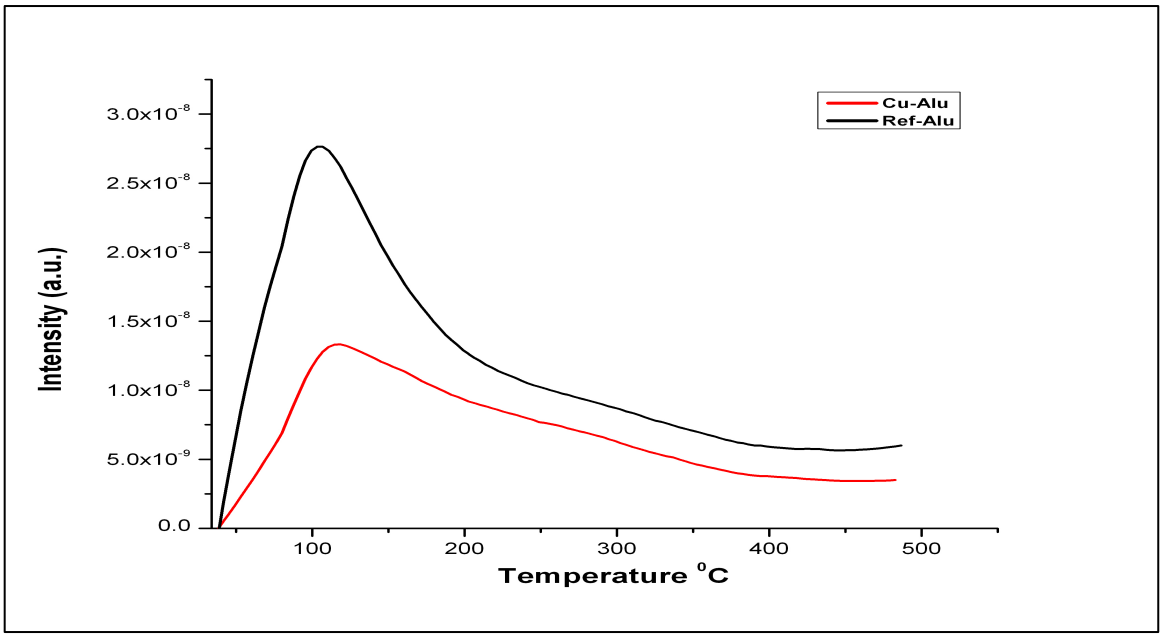

Figure 2.3 Ammonia Temperature-Programmed Desorption (NH_3-TPD) profiles of both Cu-Alu and Ref-Alu samples.

Table 2.2 The Calculated Peak Area of Cu-Alu and Ref-Alu Samples

Catalyst Type	Peak Area (10^5)
Cu-Alu	0.31
Ref-Alu	0.52

On the other hand, the Cu-Alu sample has a smaller ammonia desorption peak at the same range between 60 and 350 °C with a peak area of 0.31. This indicates that copper covered a portion of the support surface area and acid sites. The results from the CO-pulse reinforced this observation. The possible formation of bulk copper aluminate with an average active diameter of 12.68 nm affected the NH_3 desorption. However the overall profile of ammonia desorption looks broader than the profile of the Ref-Alu sample. This suggests that some of the copper species worked as adsorption sites. In fact, this could increase the NH_3 adsorption capacity of the Cu/Alu catalyst and this is important since the NH_3-SCR reaction is mainly based on the adsorption of ammonia.

However, The NH_3-TPD alone cannot distinguish between Lewis and Brønsted acid sites. In fact, the TPD temperature peak is used as a rough measure of the acid strength of the adsorption sites; it can distinguish sites by adsorption strength only, but not Lewis from Brønsted sites. It is like an overall measurement of the acid strength.

2.5.4 Temperature-Programmed Desorption Analysis of (NH_3, NO and Combined NH_3-NO)

This subsection provides a study of selected species N_2, NO, NH_3 and N_2O from three different TPD tests with NH_3, NO and NH_3/NO. The aim of this study was to evaluate Cu-Alu catalytic activity under three different conditions. It is important to understand how the above species behave when the catalyst is exposed to ammonia only, nitric oxide

only and combined NH_3-NO gas. This analysis might predict and estimate the generated products from an actual SCR reaction. All the data were recorded via the mass spectrometer and the peak area of different species are shown in Table 2.3.

Table 2.3 The Calculated Peak Area of Different Species Over The Cu/Alu Catalyst

Species / Test	NH_3 (10^5)	NO (10^5)	N_2O (10^5)	N_2 (10^5)
NH_3-TPD	0.31	0.16	0.05	0.26
NO-TPD	0.00	0.04	0.03	0.00
NH_3-NO-TPD	0.28	0.14	0.00	0.18

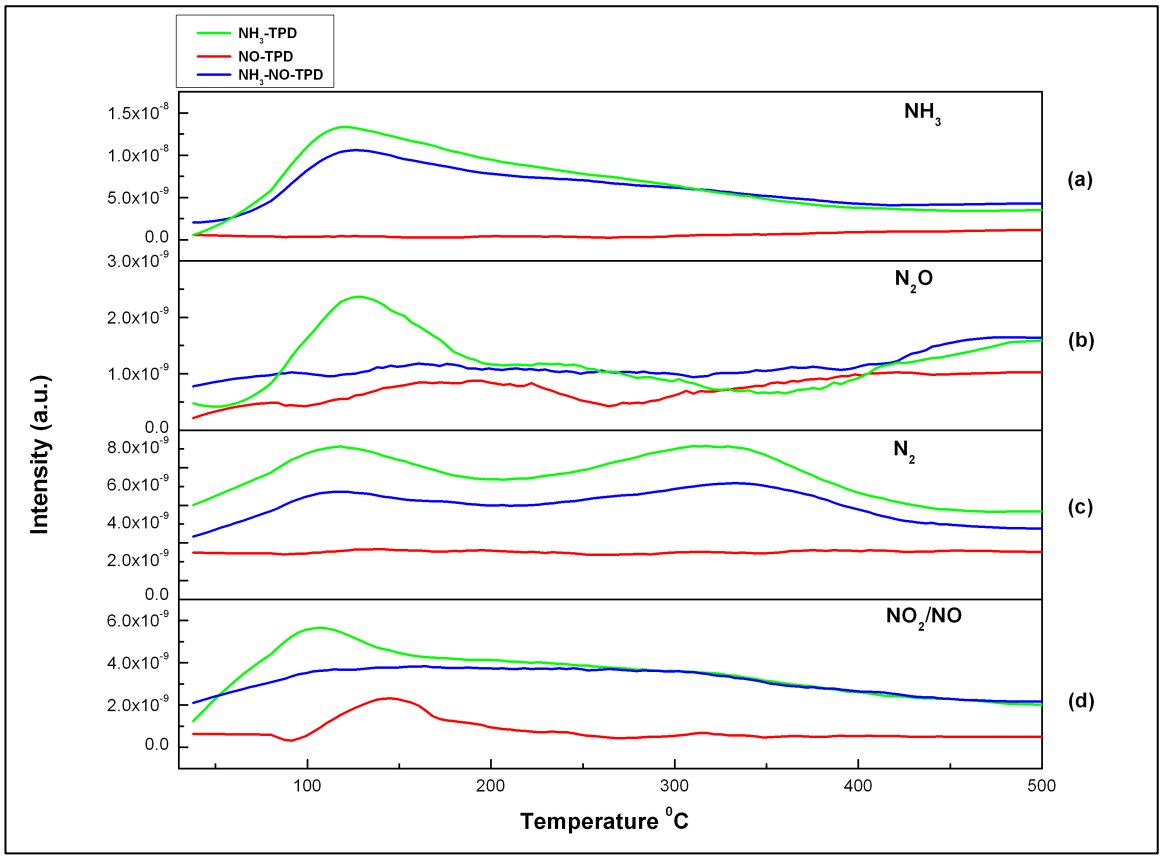

Figure 2.4 Temperature-Programmed Desorption (NH_3-TPD, NO-TPD and NH_3-NO-TPD) of the Cu-Alu catalyst, (a) NH_3 intensity signal, (b) N_2O intensity signal, (c) N_2 intensity signal, (d) NO_2/NO intensity signal.

In Fig. 2.4d, the NH_3-TPD results show a moderate amount of desorbed NO molecules from the catalyst surface with a peak area of 0.16. NO could be formed when NH_3 reacted with oxygen (reaction 2.1) during the ammonia saturation step prior to the TPD test.

$$4NH_3 + 5O_2 \rightarrow 4NO + 6H_2O \quad (2.1)$$

The NO-TPD and NH_3-NO-TPD results show obvious NO desorption peaks. The sharp NO peak from the NO-TPD test has a peak area of 0.04. On the other hand, the NO desorption peak area from the NH_3-NO-TPD test was 0.14. It was much broader and larger than the peak from the NO-TPD. In fact, the NH_3 dose might enhance NO adsorption on the catalyst surface.

In the case of the N_2 species, Fig. 2.3c exhibits the nitrogen desorption curves of three TPD tests. The desorbed nitrogen from both NH_3-TPD and NH_3-NO-TPD tests could be produced via the oxidation of NH_3 (reaction 2.2). These desorption profiles appeared to be broad and wide. It is believed that reduced copper created more active sites and this enhanced the adsorption. However, there was no nitrogen desorption peak from NO-TPD. This implies that the catalyst needs a reducing agent to convert NO to N_2.

$$4NH_3 + 3O_2 \rightarrow 2N_2 + 6H_2O \quad (2.2)$$

The MS signals of nitrous oxide are represented in Fig. 2.3b. No N_2O desorption peaks were observed for both NO-TPD and NH_3-NO-TPD tests. In the absence of ammonia, the catalyst is inactive and N_2O could not be generated as seen from

the NO-TPD tests. For NH_3-NO-TPD, in the presence of a small amount of oxygen and ammonia, the reaction tended to produce more N_2 and H_2O according to reaction 2.3. However, N_2O peak from the NH_3-TPD test is much more obvious than the others. The oxidation of NH_3 to N_2O (reaction 2.4) could occur due to the existence of O_2 and NH_3.

$$4NH_3 + 4NO + O_2 \rightarrow 4N_2 + 6H_2O \quad (2.3)$$

$$2NH_3 + 2O_2 \rightarrow N_2O + 3H_2O \quad (2.4)$$

NH_3 desorption peaks from TPD tests are shown in Fig. 2.4a. The peak area of ammonia from the NH_3-TPD test was the largest, 0.31, due to the fact that NH_3 was the only injected gas and it covered most of active sites. However, the ammonia peak area from NH_3-NO-TPD results was 0.28, small comparing to the NH_3-TPD results. The results indicate that the competitive adsorption of two different gases happened on the catalyst surface.

On the other hand, no NH_3 peak was shown from the NO-TPD results. It appears that during the TPR experiment, all the ammonia might be removed.

Overall, the Cu-Alu catalyst was able to adsorb different species. More importantly, it was able to adsorb both NH_3 and NO on its surface. These two are the main reactants during the SCR reactions. Moreover, the adsorption peak temperature ranges of most species were wide (about 50-400 °C). This indicates that the interaction strength of active sites with reactants on the Cu-Alu catalyst has a wide range and this is beneficial for the catalyst to have a wide operating temperature range.

CHAPTER 3

Cu/SAPO-34

3.1 Silicoaluminophosphate Molecular Sieve (SAPO-34)

SAPO-34 has a zeolite structure. Its framework combines Si, Al and P as tetrahedral atoms linked together with oxygen atoms in between (Fig. 3.1). SAPO-34 is a crystalline, microporous zeotype that shares topology with the mineral chabazite (CHA), where micropores are smaller than 2 nm [57]. SAPO-34 is known as a small-pore zeolite. Like other zeolites, it is three-dimensional (Fig. 3.1). As other microspore materials are designated with large specific surface areas, SAPO-34 has a pronounced specific surface area up to 550 m^2/g [57]. It has the chabazite structure where twisted hexagonal prisms are linked together by four-member rings resulting in large, elliptical cavities, which are known as cages. Furthermore, each cage makes a group of 7 cages linked by the 8-member oxygen rings [58, 59]. The dimensions of a single cage are 0.75 nm in diameter and 0.82 nm high, whereas, the 8-member oxygen rings have 0.38 in diameter and 0.43 nm in size [60, 61].

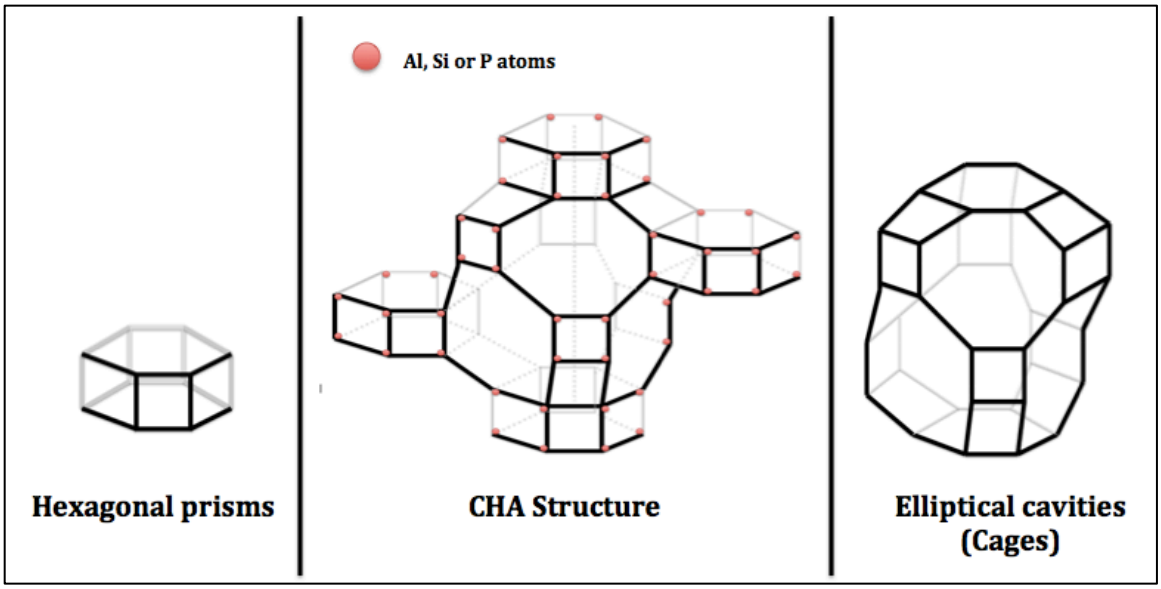

Figure 3.1 SAPO-34 framework structures.

Source: Sørli, G., Effect of Porosity on the Hydrothermal Stability of Cu/SAPO-34 for the deNOx Process. 2016: NTNU. p. 115.

3.2 SAPO-34 Supported Copper Catalyst (Cu/SAPO-34)

SAPO-34 has been attracting much attention in different catalytic applications due to its small-pore feature. The pores of SAPO-34, created via the 4-member rings, 6-member-rings and the 8-member rings, can function as molecular sieves [57]. SAPO-34 is extensively studied in the catalytic reaction of converting methanol to olefin (MTO) [60, 61]. In this case, SAPO-34 worked as a catalyst for the (MTO) reaction and it was shown to be a robust catalyst for the conversion, particularly to lighter olefins due to its selectivity. Moreover, SAPO-34 could be used as a support due to its medium acidic strength. For the NH_3-SCR reaction, the SAPO-34 supported copper provides acidic sites for NH_3 adsorption and activation to further react with NO_X species [62].

In a recent study, Cu/SAPO-34 was able to maintain the optimum deNOx activity of about 90 -100% at temperature between (250–450 °C) and even after hydrothermal aging

at 800 °C with high NO_X conversion [34, 35]. Another study [63] found that SAPO-34 (small-pore zeotype) supported copper catalyst had better SCR activity and more hydrothermal stability than Cu/ZSM-5 catalyst (medium pore zeolite).

3.3 Preparation of Copper-Silicoaluminophosphate Catalyst (Cu/SAPO-34)

Both Cu/Al_2O_3 and Cu/SAPO-34 catalysts were prepared with the same preparation procedure that was discussed in subsection (2.1.3) except for one additional step. Prior to adding $Cu(NO_3)_2$ solution into the support of H-SAPO-34, H-SAPO-34 was exposed to 10 vol.% NH_3/He at 120 °C for 2 h to convert H-SAPO-34 to NH_4-SAPO-34. This stabilizing step is crucial due to the fact that SAPO-34 materials can become unstable when these materials are exposed to moisture or humid environments below 100 °C [64]. This leads to a huge decreasing in the available surface area. The 3.5 wt.% Cu/SAPO-34 was donated as Cu-SAP.

3.4 Catalyst Characterization

All TPD, TRP and the CO pulse tests were performed according to the methods explained in subsections (2.1.4.1, 2.1.4.2 and 2.1.4.3).

3.5 Results and Discussions

3.5.1 Catalyst Dispersion (CO Pulse Experiments)

Table 3.1 shows Cu-SAP results from CO-pulse test. The metal dispersion of this catalyst was 9.7%. This percentage remains low and the presence of agglomerated Cu species on the surface is possible.

On the other hand, the active phase diameter (10.67nm) further confirms the low metal dispersion. This indicates that the impregnated Cu species on the surface could be as crystallites, CuO or other large size Cu species.

Table 3.1 Details of Cu Dispersion, Cu Particle Size

Sample	Metal dispersion (%)	Active Particle Diameter (nm)
Cu-SAP	9.7	10.67

3.5.2 H_2-TPR Analysis

An overall idea of the copper species can be identified from the TPR experiment. Fig. 3.2 shows a single reduction peak of Cu-SAP from 210 to 280 °C with a peak maxima at 230 °C. In fact, there is unfortunately no real agreement regarding the identification of this peak. For instance, a previous study [65] observed a similar H_2 consumption peak on an ion- exchanged Cu-SAPO-34 catalyst. The low temperature peak was assigned to be either isolated Cu^{2+} or CuO. However, another study [66], used a similar catalyst, Cu exchanged SAPO-34, and reported that the low temperature H_2 consumption was assigned to the reduction of CuO clusters on the external surface of SAPO-34. In fact, assigning H_2 consumption peaks to various Cu species is based on different factors, but generally speaking, the low-temperature peaks were assigned to the reduction of isolated

Cu^{2+} to Cu^{+} ions and CuO to Cu^{0} [67].

Regarding our data, the Cu-SAP could have both isolated Cu^{+} and CuO species. And, this is in agreement with a recent study [68] where a Cu-SAPO-34 catalyst prepared by an impregnation method consisted of the two species: isolated Cu^{+} and CuO. Furthermore, the CO chemisorption results show a Cu species with a large diameter around 10.67 nm. Therefore, the TRP peak could be assigned to the two species but further experiments are needed to confirm this conclusion.

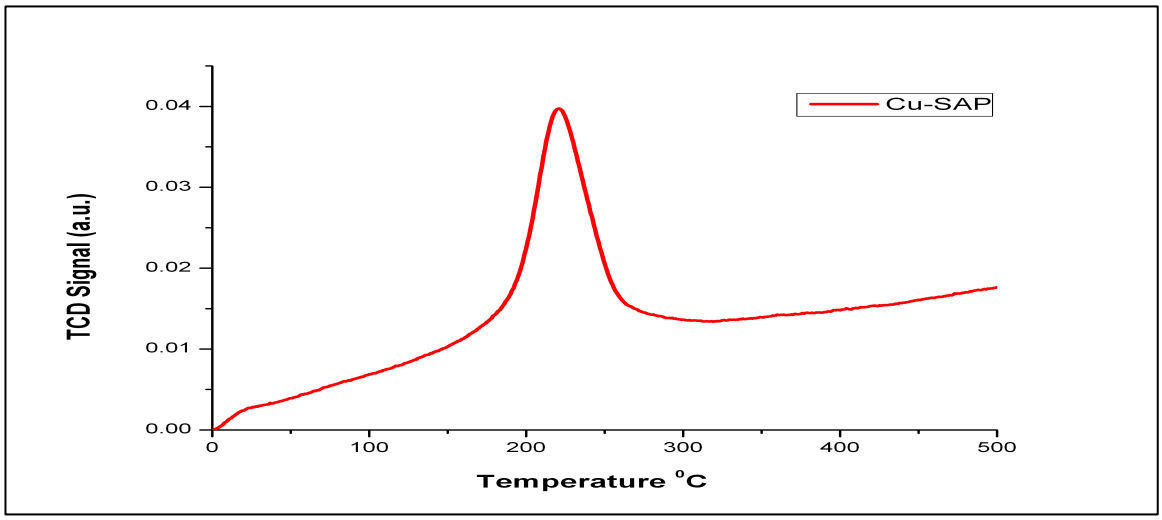

Figure 3.2 Temperature-Programmed Reduction (TPR) for Cu-SAP catalyst.

3.5.3 NH_3-TPD Surface Acidity

It is known that the catalyst surface acidity influences the SCR activity [69]. In this study, the acid properties of both Cu-SAP and Ref-SAP were studied via NH_3-TPD experiments. Also, NH_3 has been recognized as an efficient probe molecule to characterize zeotype structure acidity [70]. Fig. 3.4 displays the NH_3 desorption profiles for both samples. In fact, three NH_3 desorption peaks were evident in the NH_3-TPD

results. The Ref-SAP sample has a low temperature (LT) peak at 91.29 °C, a high temperature peak (HT) at 451.59 °C and a medium temperature peak (MT) at 175.62 °C, whereas the Cu-SAP has LT, HT and MT peaks at 95.12,183.28 and 424.76 °C, respectively. In fact, these NH_3 desorption peaks were formed from the adsorption of NH_3 on the catalyst surface that has different acid strengths [36, 66]. However, the assessment of these features is not straightforward and could not be identified with the TPD test only, but it can be noticed that these samples have acidic sites with a broad temperature range. This can increase the ammonia adsorption process.

The Cu-SAP profile (shown in Fig. 3.3) is similar to the Ref-SAP profile but with a weaker intensity. Comparing Ref-SAP with Cu-SAP (Table 3.2), the peak area for Ref-SAP sample (4.74) was greater than that from Cu-SAP (1.67). It has more acid sites. This major decrease in acid sites after Cu loading is possibly due to the fact that Cu loading covered some acid adsorption sites and SAPO-34 structure collapsed during the synthesis. This also indicates that the surface acidity of Cu/SAPO-34 comes mainly from the SAPO-34 support [66]. Looking at the (MT) region in Fig. 3.4 for both samples, the Cu-SAP has a little broader profile compared to the Ref-SAP sample. This suggests that Cu species created adsorption sites for ammonia. It is believed that the center of the active metal functions as an acidic surface adsorbing more NH_3 species and this observation is consistent with the other study [71].

Table 3.2 The Calculated Peak Area for Both Cu-SAP and Ref-SAP Samples

Catalyst Type	Peak Area (10^5)
Cu-SAP	1.67
Ref-SAP	4.74

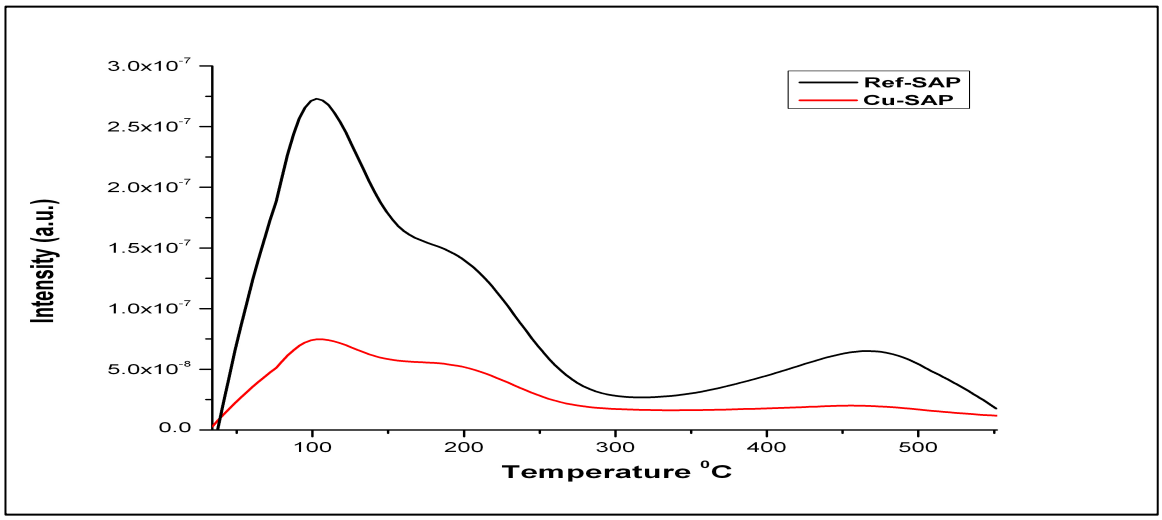

Figure 3.3 NH_3-TPD for Cu-SAP and Ref-Alu samples.

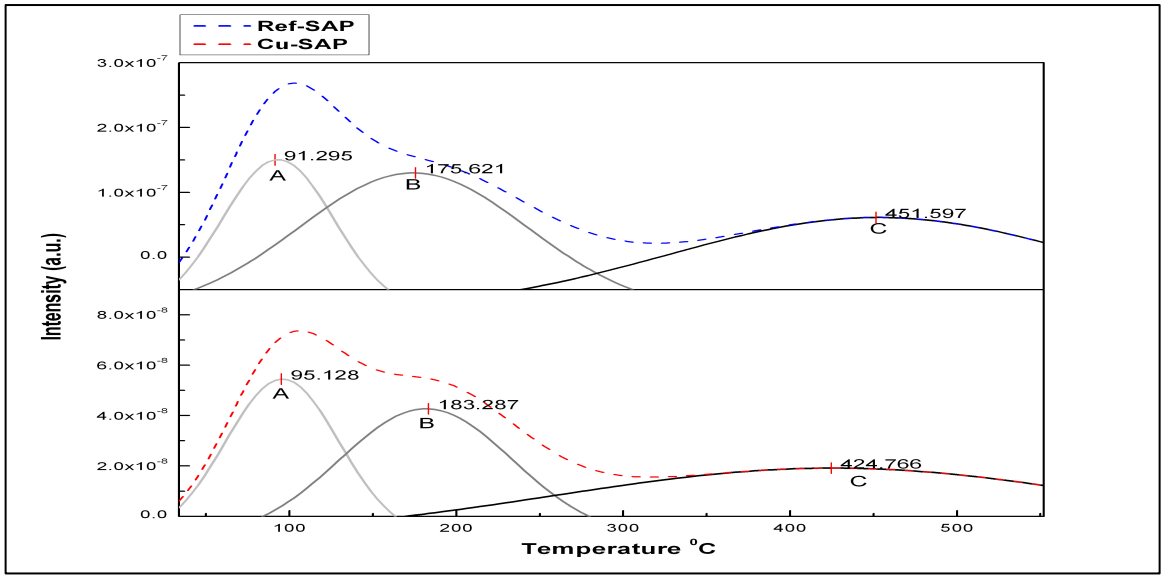

Figure 3.4 NH_3-TPD for Cu-SAP and Ref-Alu represents LT and MT and HT peaks.

3.5.4 Temperature-Programmed Desorption Analysis of NH_3, NO and Combined NH_3-NO

Fig. 3.5a, displays the NH_3 desorption profiles of the three tests. The desorbed ammonia profiles for NH_3-TPD, and NH_3-NO-TPD experiments show pronounced peaks with peak areas of 1.67 and 1.62, respectively. These two areas are almost equal and also have the

same profile. This indicates that the Cu-SAP catalyst could adsorb ammonia when the catalyst was exposed to NH_3 and NO.

In Fig. 3.5c, no intense N_2O signals are shown from these experiments. Only a very small low intensity N_2O peak with an area of 0.32 is noticed when the two gases flowed simultaneously. This could be formed from the reaction 3.1 prior to the TPD test. And, the reduction in oxygen intensity (shown in Fig. 3.5b) and the increase in H_2O intensity (shown in Fig. 3.5f) reinforce this conclusion.

$$2NH_3 + 2O_2 \rightarrow N_2O + 3H_2O \quad (3.1)$$

Table 3.3 The Calculated Peak Area of Different Species Over the Cu/SAP Catalyst

Species / Test	NH_3 (10^5)	H_2O (10^5)	NO (10^5)
NH_3-TPD	1.67	1.58	0.31
NO-TPD	0.00	0.00	0.10
NH_3-NO-TPD	1.62	0.78	0.30

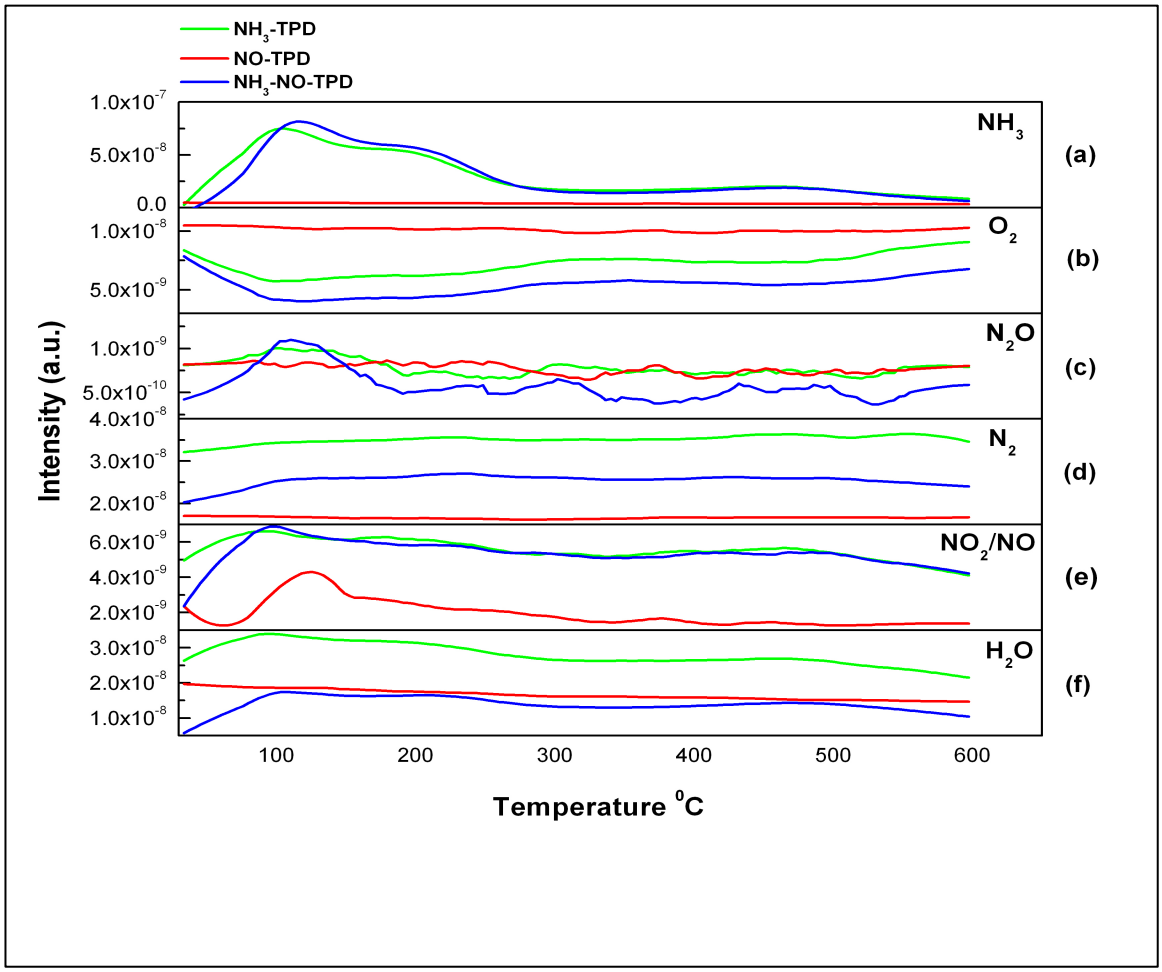

Figure 3.5 Temperature-Programmed Desorption (NH_3-TPD, NO-TPD and NH_3-NO-TPD) of Cu-SAP Catalyst, (a) NH_3 intensity signal, (b) O_2 intensity signal, (c) N_2O intensity signal, (d) N_2 intensity signal, (e) NO_2/NO intensity signal, (f) H_2O intensity signal.

Similarly, there is a weak N_2 signal from both NH_3-TPD and NH_3-NO-TPD experiments, N_2 is produced from the reaction 3.2. The increase in H_2O and the decrease in O_2 intensity signals (Fig. 3.5f and Fig. 3.5b respectively) further support this observation.

$$4NH_3 + 3O_2 \rightarrow 2N_2 + 6H_2O \qquad (3.2)$$

From Fig. 3.5e, the NH_3-TPD profile shows a desorbed NO peak with an area of 0.31. This amount of NO might be produced from the reaction 3.3.

$$4NH_3 + 5O_2 \rightarrow 4NO + 6H_2O \quad (3.3)$$

For the NO-TPD test, a single sharp NO peak with an area of 0.10 is observed. It indicates that the adsorption sites for NO are similar. For the NH_3-NO-TPD test, the NO peak (with area of 0.30) is much broader and larger compared to the NO-TPD result. It implies that NH_3 might enhance NO adsorption on the catalyst surface.

CHAPTER 4

Cu-SAP vs. Cu-Alu

4.1 Comparison Between Cu-SAP vs. Cu-Alu

4.1.1 Catalyst Dispersion (CO Pulse Experiments)

From Table 4.1, it is clearly seen that both Cu dispersion and Cu particle size for the two catalysts are quite similar. The copper species over both surfaces were not well dispersed. Also, these copper species were different in size. These findings suggest that the agglomerated species might cover the available sites and this could affect the adsorption of both NH_3 and NO. The NH_3-TPD results reinforced that observation. The adsorption peaks of Cu-SAP and Cu-Alu are much smaller than the Ref-SAP and Ref-Alu samples.

Table 4.1 Cu Dispersion and Cu Particle Size Comparison

Catalyst	Metal dispersion (%)	Active Particle Diameter (nm)
Cu-Alu	8	12.68
Cu-SAP	9.7	10.67

4.1.2 H_2-TPR Analysis

Based on the H_2-TPR analysis of Cu-Alu and Cu-SAP catalysts (subsections: 2.1.5.2 and 3.1.5.2), the Cu-Alu surface could have two Cu species: a copper aluminate surface phase ($CuAl_2O_4$) and a bulk copper aluminate whereas, the isolated Cu^{+2} and CuO clusters species could be found on the Cu-SAP surface. Generally speaking, the large size Cu contents like bulk copper aluminate and CuO are not effective for the SCR reaction. For instance, during the low temperature operation, CuO does not contribute to the SCR activity and this species negatively impacts SCR activity at the high temperature ranges

due to NH_3 over-oxidation [72]. Furthermore, increasing Cu loading promotes the formation of surface CuO clusters and CuO crystallites [73]. In our case, about 4.2 wt.% and 3.5 wt.% of Cu were used in the catalyst synthesis. One study used SAPO-34 with different Cu loading (1.5 to 3 wt.%) catalysts for the SCR system. They noticed that the increase in Cu loading led to an increase of CuO species [66].

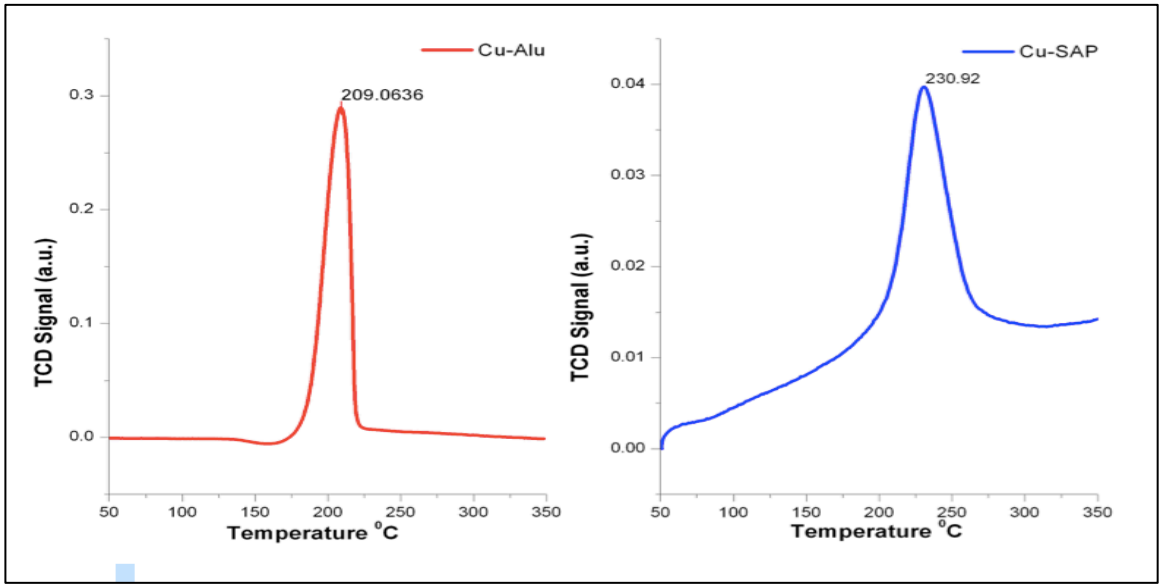

Figure 4.1 Temperature-Programmed Reduction (TPR) for Cu-SAP and Cu-Alu catalysts.

4.1.3 NH_3-TPD Surface Acidity

Table 4.2 displays the peak area for Cu-SAP and Cu-Alu catalysts, 1.55 and 0.31 respectively. The adsorption peak area of Cu-SAP is about 5 times the Cu-Alu peak area. Besides, the Cu providing adsorption sites, the high adsorption capacity of Cu-SAP could be associated to two reasons. The first reason is that the porous structure of SAPO generated a huge surface area that can adsorb more ammonia than alumina does. The other reason is that the SAPO structure is able to greatly adsorb ammonia at a wide

temperature range (three peaks of adsorption). Thus, Cu-SAP could be more effective than Cu-Alu for the SCR reaction.

Table 4.2 The Calculated Peak Area for Both Cu-SAP and Ref-SAP Samples

Catalyst Type	Peak Area (10^5)
Cu-SAP	1.67
Cu-Alu	0.31

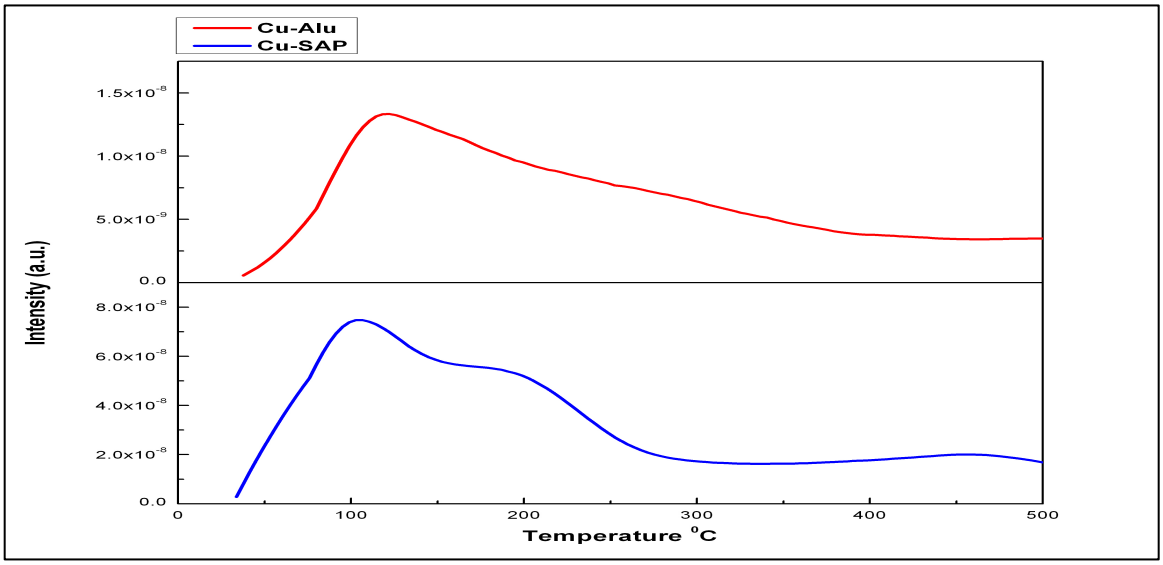

Figure 4.2 NH_3-TPD for Cu-SAP and Cu-Alu samples.

4.1.4 Temperature-Programmed Desorption Analysis of NH_3, NO and Combined NH_3-NO

Fig. 4.3.a displays the NO desorption peaks of the two catalysts from NO-TPD-. It is obvious that the peaks of the two catalysts are similar. Table 4.3 lists the peak areas. For the Cu-Alu peak, the area is 0.04 while the peak area of Cu-SAP is 0.10. It indicates that NO adsorption for both Cu-Alu and Cu-SAP catalysts are weak without ammonia being adsorbed first on the surface. However, once the ammonia is present on the surface (Fig. 4.3.b), obvious NO desorption peaks are shown for Cu-Alu and Cu-SAP with increased

peak areas of 0.14 and 0.30, respectively. These findings suggest that both catalysts would be efficient for NH_3-SCR due to their capability to adsorb NO in the presence of NH_3.

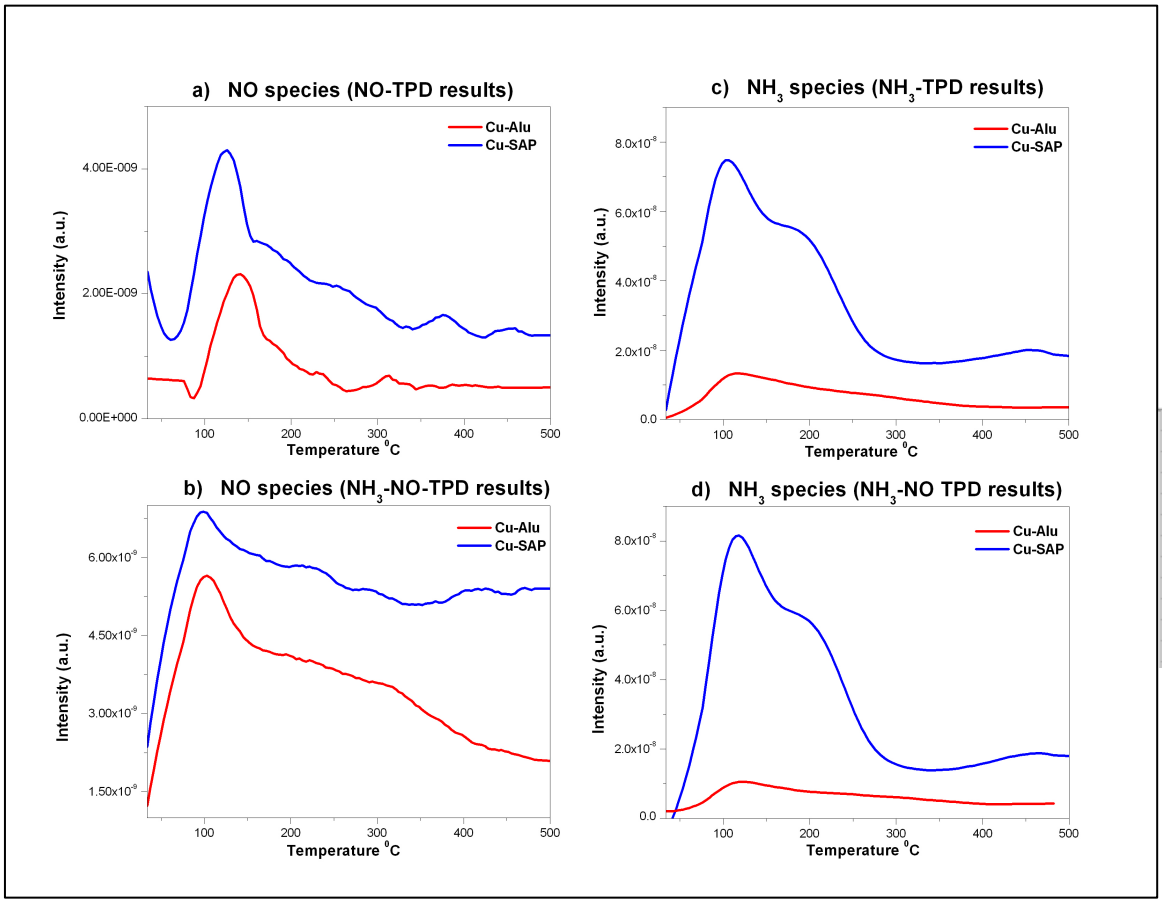

Figure 4.3 Desorbed species from (NH_3-TPD, NO-TPD and NH_3-NO-TPD) of Cu-Alu and Cu-SAP catalysts, (a) NO intensity signal from NO-TPD-Only, (b) NO intensity signal from NH_3-NO-TPD, (c) NH_3 intensity signal from NH_3-TPD-Only, (d) NH_3 intensity signal from and NH_3-NO-TPD.

For the adsorption of NH_3 shown in Fig. 4.3.c and Fig. 4.3.d, the Cu-SAP catalyst shows pronounced NH_3 peaks with very significant areas (1.67 for NH_3-TPD & 1.62 for combined NH_3-NO-TPD. On the other hand, the Cu-Alu capacity was way too small with an average peak area of 0.295. In fact, the influence of the support plays a major role in

case of ammonia adsorption. The SAPO is a porous material with a surface area up to 550 m^2/g, providing an enormous surface area. Furthermore, its zeotype structure provides a strong acidity along with wide temperature range. Thus, Cu supported on SAPO-34 could enhance the NH_3-SCR reaction due to its significant ammonia adsorption capacity.

Table 4.3 The Calculated Peak Area of Different Species Over The Cu/SAP Catalyst and Cu-Alu

Species / Catalyst	NH_3		NO	
	NH_3-TPD (10^5)	NH_3-NO-TPD (10^5)	NO-TPD (10^5)	NH_3-NO-TPD (10^5)
Cu/SAP	1.67	1.62	0.10	0.30
Cu-Alu	0.31	0.28	0.04	0.14

4.2 Future Work

Cu/SAPO-34 and, Cu/Al_2O_3 catalysts suffered from losing a huge surface area compared to the SAPO-34 and Al_2O_3 materials (confirmed via NH_3-TPD). Performing additional test such as a Brunauer–Emmett–Teller (BET) experiment would give important information about the available surface area before and after adding copper. And, this is crucial to find the actual surface area to determine whether the loss of surface is due to the formation of agglomerated copper species blocking the catalyst surface or other problems related to operating conditions and catalyst synthesis.

Another important characterization is X-Ray Diffraction (XRD). It is used to identify sample composition, species phase, and crystallite size. In our case, this could be used to see if the SAPO-34 or Al_2O_3 structures were collapsed after the impregnating of Cu. Furthermore, we can find the compositions and the phases of copper, verify whether

the formation of undesirable CuO or bulk Cu aluminate could block the acid sites on the surface.

Besides, finding the possible interpretation of the surface area problem via characterization tests and changing the catalyst synthesis method from incipient wetness impregnation to an ion-exchanged method could improve the catalyst properties. In fact a recent study reported that copper ion exchanged SAPO-34 had no CuO species compared to the incipient wetness impregnation method[68]. The ion-exchanged process prevents the formation of large size copper contents, which could facilitate the adsorption of NH_3 and NO molecules on the active sites.

CHAPTER 5

CONCLUSION

In this present work, the influences of different NH_3-SCR catalyst supports (Al_2O_3 and SAPO-34) were investigated for NO and NH_3 adsorption. Both catalysts, Cu/Al_2O_3 and Cu/SAPO-34 were prepared by an incipient wetness impregnation method. Temperature programmed desorption experiments of NH_3, NO and combined NH_3-NO gases were examined to evaluate the adsorption of NO and NH_3. Cu/SAPO-34 showed a very strong NH_3 peak compared to the ammonia desorption peak of Cu/Al_2O_3. This improvement in ammonia adsorption capacity has a direct relation with the SAPO-34 surface area and its strong acidity for a wide temperature range. Furthermore, the NO adsorptions over Cu/Al_2O_3 and Cu/SAPO-34 were relatively similar. Both showed very small sharp desorption peak when only NO flowed over the catalysts, but the peaks became broader and pronounced once NO was combined with NH_3 gas.

However, comparing the surface acidity between both (Cu/Al_2O_3 & Cu/SAPO-34) with their supports (Al_2O_3 & SAPO-34), there was a dramatic decrease in the surface area and its acidity. Both TPR results and CO pulse data confirmed the formation of bulk and clusters Cu species. These large species might cover or hide the acidic spots on the support.

REFERENCES

1. OICA. *Worldwide automobile production from 2000 to 2015 (in million vehicles)*. In Statista - The Statistics Portal n.d. Feb. 20, 2017]; Available from: https://www.statista.com/statistics/262747/worldwide-automobile-production-since-2000/.

2. Administration, U.S.E.I. *Projected growth in CO2 emissions driven by countries outside the OECD*. 2016 Feb. 20, 2017]; Available from: http://www.eia.gov/todayinenergy/detail.php?id=26252.

3. Armor, J.N., *Review: Environmental catalysis.* Applied Catalysis B, Environmental, 1992. **1**: p. 221-256.

4. Roy, S., M.S. Hegde, and G. Madras, *Catalysis for NOx abatement.* Applied Energy, 2009. **86**(11): p. 2283-2297.

5. AirNow. *Good Up High Bad Nearby - What is Ozone?*. 2003 [cited Feb. 20, 2017; Available from: https://cfpub.epa.gov/airnow/index.cfm?action=gooduphigh.index.

6. Information, N.C.f.B. *PubChem Compound Database*. n.d. Feb. 20, 2017]; Available from: https://pubchem.ncbi.nlm.nih.gov/compound/948.

7. Bosch, H., Janssen, F., *Catalytic Reduction of Nitrogen Oxides.* Catal. Today, 1988. **Volume 2**: p. Page 369.

8. Whatsyourimpact. *What are greenhouse gases?* Greenhouse gases n.d. Feb 20.2017]; Available from: http://whatsyourimpact.org/greenhouse-gases.

9. Greenfacts. *Air Pollution Nitrogen Dioxide*. n.d. Feb. 20, 2017]; Available from: http://www.greenfacts.org/en/nitrogen-dioxide-no2/level-2/01-presentation.htm - 0.

10. Woodford, C. *Diesel engines*. 2009 Feb. 20, 2017]; Available from: http://www.explainthatstuff.com/diesel-engines.html.

11. DieselNet. *Emission standards*. Summary of worldwide engine emission standards n.d. Feb. 21, 2017]; Available from:https://www.dieselnet.com/standards/ - eu.

12. Bröer, S. and T. Hammer, *Selective catalytic reduction of nitrogen oxides by combining a non-thermal plasma and a V2O5-WO3/TiO2 catalyst.* Applied Catalysis B: Environmental, 2000. **28**(2): p. 101-111.

13. Skalska, K., J.S. Miller, and S. Ledakowicz, *Trends in NOx abatement: A review.* Science of The Total Environment, 2010. **408**(19): p. 3976-3989.

14. Han, J., et al., *Urea-SCR catalysts with improved low temperature activity.* SAE Technical Papers, 2011.

15. Chou, T.S., *FCC process with fines tolerant SCR reactor*. 1995, Google Patents.

16. Cheng, X. and X.T. Bi, *A review of recent advances in selective catalytic NOx reduction reactor technologies.* Particuology, 2014. **16**: p. 1-18.

17. Johnson, T.V., *Vehicular Emissions in Review.* SAE Int. J. Engines, 2012. **5**(2): p. 216-234.

18. Zhan, R., M. Li, and L. Shui, *Updating China Heavy-Duty On-Road Diesel Emission Regulations*. 2012, SAE International.

19. Fränkle, G., *The Exhaust Gas Purification System for Trucks.* Int. Wiener Motorensymposium, 1996. **18**: p. 24-25.

20. Guan, B., et al., *Review of state of the art technologies of selective catalytic reduction of NOx from diesel engine exhaust.* Applied Thermal Engineering, 2014. **66**(1–2): p. 395-414.

21. Li, Y., et al., *Novel straight synthesis of super-microporous Cu/Al2O3 catalyst with high CH4-SCR-NO activity.* Catalysis Communications, 2015. **65**: p. 6-9.

22. Liu, Z. and S. Ihl Woo, *Recent Advances in Catalytic DeNOX Science and Technology.* Catalysis Reviews, 2006. **48**(1): p. 43-89.

23. Maunula, T., et al., *Design of Durable Vanadium - SCR Catalyst Systems for Heavy - Duty Diesel Applications*. 2013, The Automotive Research Association of India.

24. Xu, C., et al., *NH3-SCR denitration catalyst performance over vanadium–titanium with the addition of Ce and Sb.* Journal of Environmental Sciences, 2015. **31**: p. 74-80.

25. Liu, Z.G., N.A. Ottinger, and C.M. Cremeens, *Vanadium and tungsten release from V-based selective catalytic reduction diesel aftertreatment.* Atmospheric Environment, 2015. **104**: p. 154-161.

26. Long, R.Q. and R.T. Yang, *Reaction Mechanism of Selective Catalytic Reduction of NO with NH3 over Fe-ZSM-5 Catalyst.* Journal of Catalysis, 2002. **207**(2): p. 224-231.

27. Blakeman, P.G., et al., *The role of pore size on the thermal stability of zeolite supported Cu SCR catalysts.* Catalysis Today, 2014. **231**: p. 56-63.

28. Brandenberger, S., et al., *The State of the Art in Selective Catalytic Reduction of NOx by Ammonia Using Metal–Exchanged Zeolite Catalysts.* Catalysis Reviews, 2008. **50**(4): p. 492-531.

29. Beutel, T., et al., *Redox Chemistry of Cu/ZSM-5.* The Journal of Physical Chemistry, 1996. **100**(2): p. 845-851.

30. Yan, J.Y., et al., *Deactivation of Cu/ZSM-5 Catalysts for Lean NOxReduction: Characterization of Changes of Cu State and Zeolite Support.* Journal of Catalysis, 1996. **161**(1): p. 43-54.

31. Iwamoto, M., et al., *Removal of nitrogen monoxide through a novel catalytic process. 1. Decomposition on excessively copper-ion-exchanged ZSM-5 zeolites.* The Journal of Physical Chemistry, 1991. **95**(9): p. 3727-3730.

32. Cavataio, G., et al., *SAE Technical Paper 2007-01-1575, 2007.* 2007: p. 776-790.

33. Kwak, J.H., et al., *Excellent activity and selectivity of Cu-SSZ-13 in the selective catalytic reduction of NOx with NH3.* Journal of Catalysis, 2010. **275**(2): p. 187-190.

34. Ma, L., et al., *Characterization of commercial Cu-SSZ-13 and Cu-SAPO-34 catalysts with hydrothermal treatment for NH3-SCR of NOx in diesel exhaust.* Chemical Engineering Journal, 2013. **225**: p. 323-330.

35. I. Bull, R.S.B., W.M. Jaglowski, G.S. Koermer, A. Moini, J.A. Patchett, W.M. Xue, P. Burk, J.C. Dettling, M.T. Caudle. 2009.

36. Wang, D., et al., *NH3-SCR over Cu/SAPO-34 – Zeolite acidity and Cu structure changes as a function of Cu loading.* Catalysis Today, 2014. **231**: p. 64-74.

37. Bartholomew, C.H., *Mechanisms of catalyst deactivation.* Applied Catalysis A: General, 2001. **212**(1–2): p. 17-60.

38. Forzatti, P. and L. Lietti, *Catalyst deactivation.* Catalysis Today, 1999. **52**(2–3): p. 165-181.

39. Lezcano-Gonzalez, I., et al., *Chemical deactivation of Cu-SSZ-13 ammonia selective catalytic reduction (NH3-SCR) systems.* Applied Catalysis B: Environmental, 2014. **154-155**: p. 339-349.

40. Kröger, V., *Poisoning of automotive exhaust gas catalyst components: the role of phosphorus in the poisoning phenomena*. 2007: University of Oulu.

41. Rokosz, M.J., et al., *Characterization of phosphorus-poisoned automotive exhaust catalysts.* Applied Catalysis B: Environmental, 2001. **33**(3): p. 205-215.

42. Kern, P., et al., *High-throughput study of the effects of inorganic additives and poisons on NH3-SCR catalysts. Part II: Fe–zeolite catalysts.* Applied Catalysis B: Environmental, 2010. **95**(1–2): p. 48-56.

43. Shen, M., et al., *Deactivation mechanism of SO2 on Cu/SAPO-34 NH3-SCR catalysts: structure and active Cu2+.* Catalysis Science & Technology, 2015. **5**(3): p. 1741-1749.

44. Hjuler, K. and K. Dam-Johansen, *Mechanism and kinetics of the reaction between sulfur dioxide and ammonia in flue gas.* Industrial & Engineering Chemistry Research, 1992. **31**(9): p. 2110-2118.

45. Britannica, T.E.o.E. *alumina*. 2016 Mar.17, 2017]; Available from: https://www.britannica.com/science/alumina.

46. Shirai, T., et al., *Structural properties and surface characteristics on aluminum oxide powders.* 2010.

47. Chen, L., et al., *Catalytic selective reduction of NO with propylene over Cu-Al2O3 catalysts: influence of catalyst preparation method.* Applied Catalysis B: Environmental, 1999. **23**(4): p. 259-269.

48. Sullivan, J.A. and J.A. Doherty, *NH3 and urea in the selective catalytic reduction of NOx over oxide-supported copper catalysts.* Applied Catalysis B: Environmental, 2005. **55**(3): p. 185-194.

49. Hamada, H., et al., *Transition metal-promoted silica and alumina catalysts for the selective reduction of nitrogen monoxide with propane.* Applied Catalysis, 1991. **75**(1): p. L1-L8.

50. Wolberg, A. and J.F. Roth, *Copper oxide supported on alumina.* Journal of Catalysis, 1969. **15**(3): p. 250-255.

51. Friedman, R.M., J.J. Freeman, and F.W. Lytle, *Characterization of CuAl2O3 catalysts.* Journal of Catalysis, 1978. **55**(1): p. 10-28.

52. Zhao, Q.-s., et al., *Adsorption of NO and NH3 over CuO/γ-Al2O3 catalyst.* Journal of Central South University of Technology, 2011. **18**(6): p. 1883-1890.

53. Larsson, P.-O. and A. Andersson, *Oxides of copper, ceria promoted copper, manganese and copper manganese on Al2O3 for the combustion of CO, ethyl acetate and ethanol.* Applied Catalysis B: Environmental, 2000. **24**(3–4): p. 175-192.

54. Jones, J.M., et al., *The selective oxidation of ammonia over alumina supported catalysts–experiments and modelling.* Applied Catalysis B: Environmental, 2005. **60**(1–2): p. 139-146.

55. Gang, L., et al., *Low temperature selective oxidation of ammonia to nitrogen on silver-based catalysts.* Applied Catalysis B: Environmental, 2003. **40**(2): p. 101-110.

56. Lenihan, S. and T. Curtin, *The selective oxidation of ammonia using copper-based catalysts: The effects of water.* Catalysis Today, 2009. **145**(1–2): p. 85-89.

57. Sørli, G., *Effect of Porosity on the Hydrothermal Stability of CuSAPO-34 for the deNOx Process*. 2016: NTNU. p. 115.

58. Hartmann, M. and L. Kevan, *Transition-Metal Ions in Aluminophosphate and Silicoaluminophosphate Molecular Sieves: Location, Interaction with Adsorbates and Catalytic Properties.* Chemical Reviews, 1999. **99**(3): p. 635-664.

59. Baerlocher, C., L.B. McCusker, and D.H. Olson, *Atlas of Zeolite Framework Types*. 2007: Amsterdam : Elsevier Science, 2007. 6th ed.

60. Schmidt, F., et al., *Carbon templated SAPO-34 with improved adsorption kinetics and catalytic performance in the MTO-reaction.* Microporous and Mesoporous Materials, 2012. **164**: p. 214-221.

61. Wilson, S. and P. Barger, *The characteristics of SAPO-34 which influence the conversion of methanol to light olefins.* Microporous and Mesoporous Materials, 1999. **29**(1-2): p. 117-126.

62. Wang, L., et al., *Location and nature of Cu species in Cu/SAPO-34 for selective catalytic reduction of NO with NH3.* Journal of Catalysis, 2012. **289**: p. 21-29.

63. Fickel, D.W., et al., *The ammonia selective catalytic reduction activity of copper-exchanged small-pore zeolites.* Applied Catalysis B: Environmental, 2011. **102**(3-4): p. 441-448.

64. Prasad, S., M.C. Wende, and J.L. Mohanan, *Stabilized metal-exchanged sapo material*. 2014, Google Patents.

65. Xue, J., et al., *Characterization of copper species over Cu/SAPO-34 in selective catalytic reduction of NOx with ammonia: Relationships between active Cu sites and de-NOx performance at low temperature.* Journal of Catalysis, 2013. **297**: p. 56-64.

66. Liu, X., et al., *Evolution of copper species on Cu/SAPO-34 SCR catalysts upon hydrothermal aging.* Catalysis Today, 2017. **281, Part 3**: p. 596-604.

67. Kieger, S., et al., *Selective Catalytic Reduction of Nitric Oxide by Ammonia over Cu-FAU Catalysts in Oxygen-Rich Atmosphere.* Journal of Catalysis, 1999. **183**(2): p. 267-280.

68. Yan, C., et al., *The role of isolated Cu2+ location in structural stability of Cu-modified SAPO-34 in NH3-SCR of NO.* Environ Technol, 2015. **36**(1-4): p. 169-77.

69. Schwidder, M., et al., *The role of Brønsted acidity in the SCR of NO over Fe-MFI catalysts.* Microporous and Mesoporous Materials, 2008. **111**(1–3): p. 124-133.

70. Long, R.Q. and R.T. Yang, *Temperature-Programmed Desorption/Surface Reaction (TPD/TPSR) Study of Fe-Exchanged ZSM-5 for Selective Catalytic Reduction of Nitric Oxide by Ammonia.* Journal of Catalysis, 2001. **198**(1): p. 20-28.

71. Wang, L., et al., *Role of Brønsted acidity in NH3 selective catalytic reduction reaction on Cu/SAPO-34 catalysts.* Journal of Catalysis, 2015. **324**: p. 98-106.

72. Gao, F., et al., *Structure–activity relationships in NH3-SCR over Cu-SSZ-13 as probed by reaction kinetics and EPR studies.* Journal of Catalysis, 2013. **300**: p. 20-29.

73. Pereda-Ayo, B., et al., *Role of the different copper species on the activity of Cu/zeolite catalysts for SCR of NOx with NH3.* Applied Catalysis B: Environmental, 2014. **147**: p. 420-428.